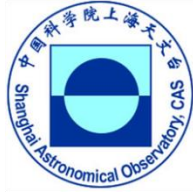




UNIVERSITY OF CHINESE ACADEMY OF SCIENCES
SHANGHAI ASTRONOMICAL OBSERVATORY

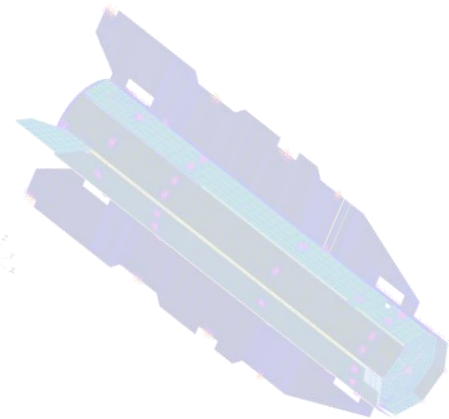


Thermospheric neutral density variations from LEO accelerometers and precise orbits

Ph.D.: Andres Calabia

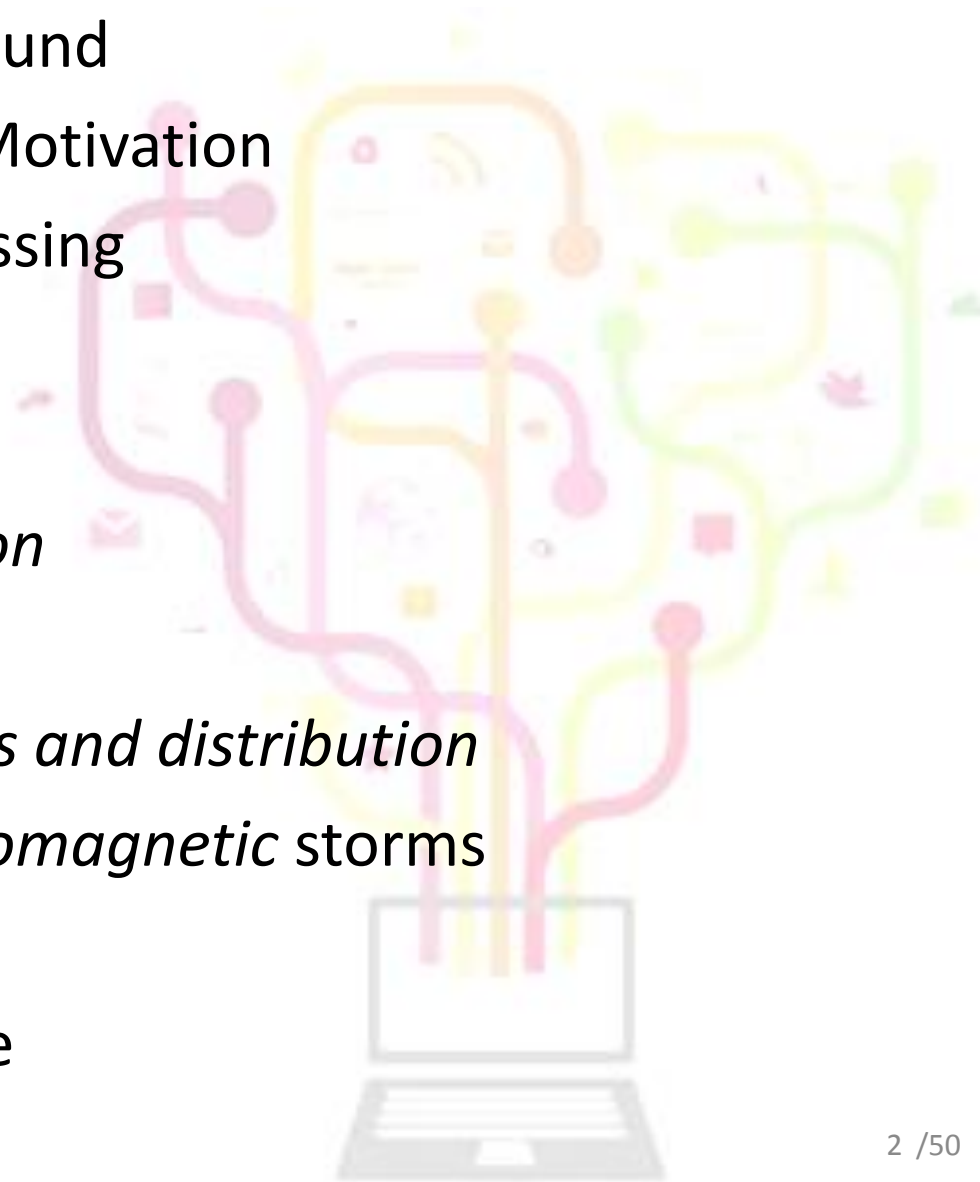
Supervisor: Prof. Shuanggen Jin

May 2017



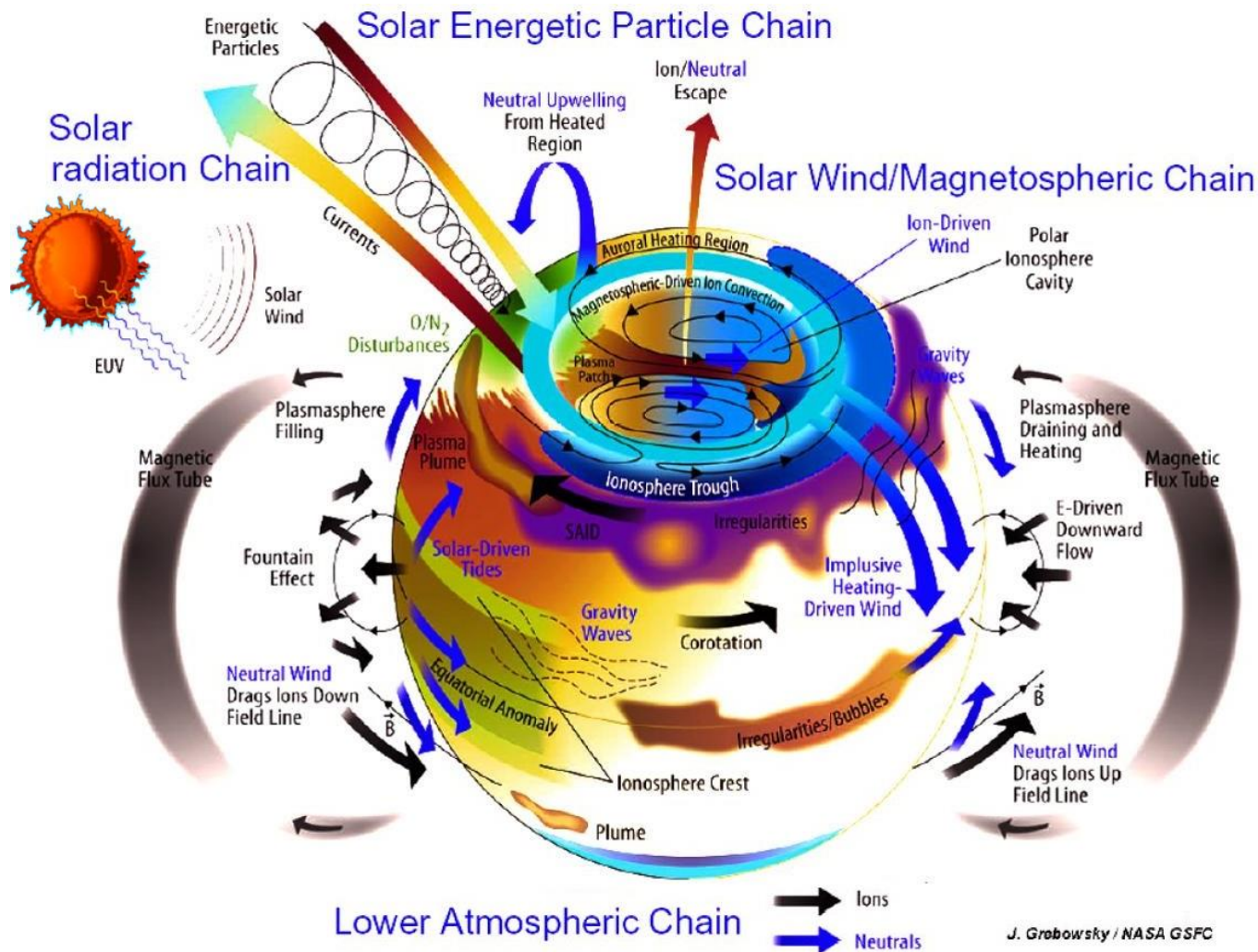
Contents

1. Introduction & Background
2. Progress, Problems & Motivation
3. Methods & Data processing
4. Results & Analysis:
 1. *POE vs ACC*
 2. *PCA parameterization*
 3. *Residuals analysis*
 4. *Long-term variations and distribution*
 5. *Variations under geomagnetic storms*
5. Conclusions
6. Problems & Perspective



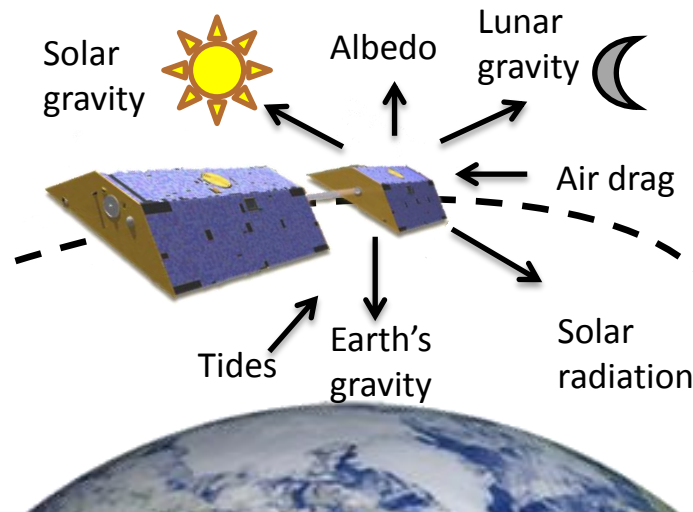
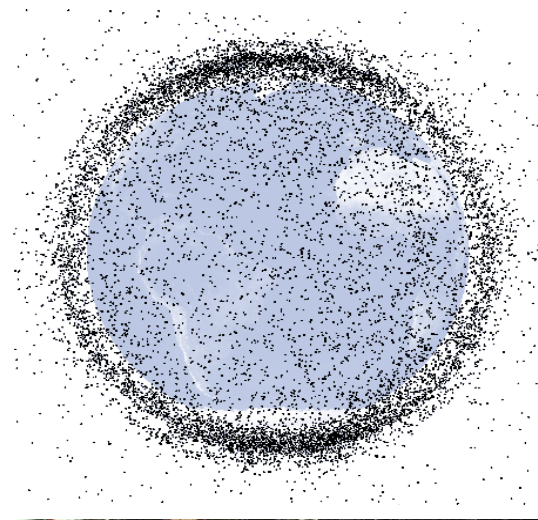
1. Introduction & Background

The thermosphere is highly ionized its geophysical processes are very complex due to the MIT coupling



1. Introduction & Background

- Half of the world's active satellites (~1000) and about 20,000 inactive debris operate in LEO, where atmospheric drag produce orbital decay and perturbations.

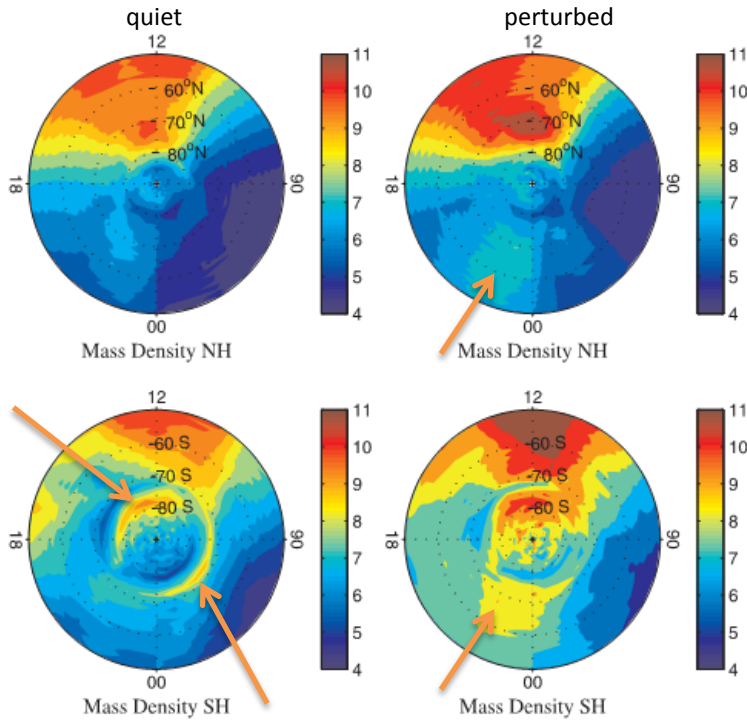


1. Introduction & Background

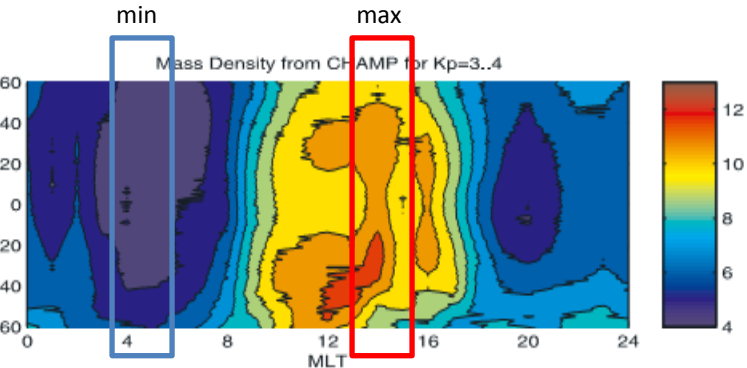
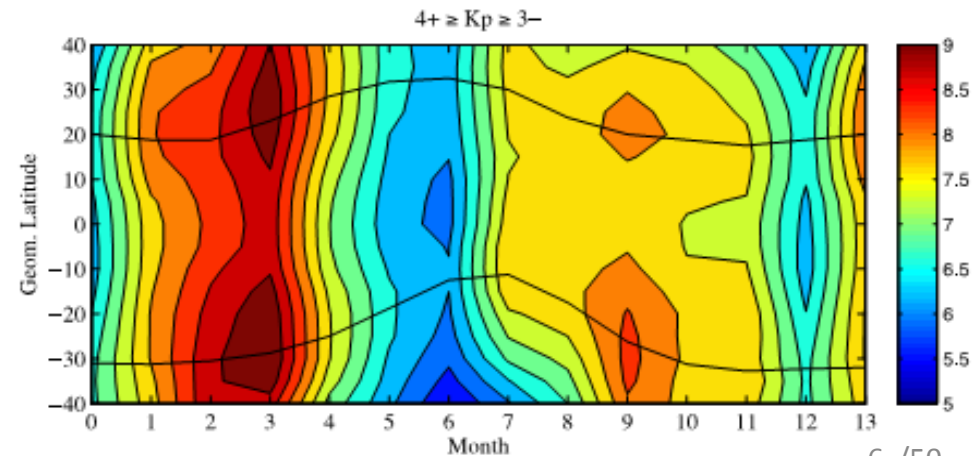
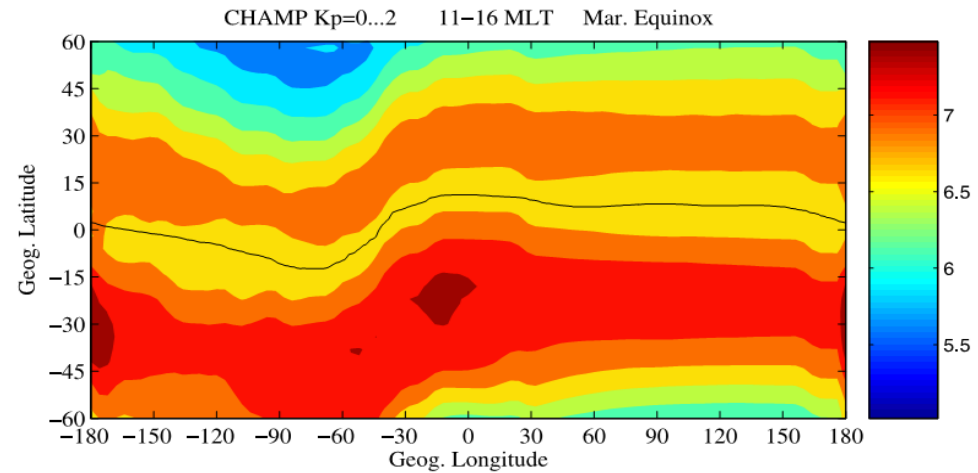
- Thermospheric neutral density measurements and models are indispensable to study the MIT coupling and its physical processes.
- Accurate air-density models are essential for ephemeris prediction, orbital tracking and satellite guidance.
- Thermospheric neutral densities can be estimated from accelerometers and GNSS onboard LEO satellites.

2. Progress, Problems & Motivation

Global distribution of the thermospheric mass density



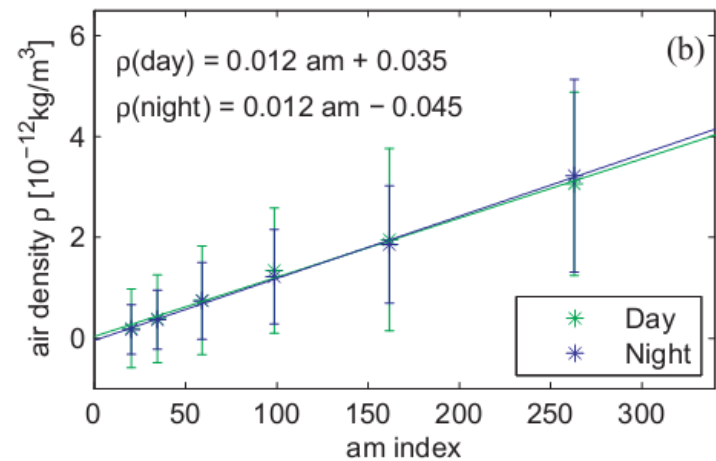
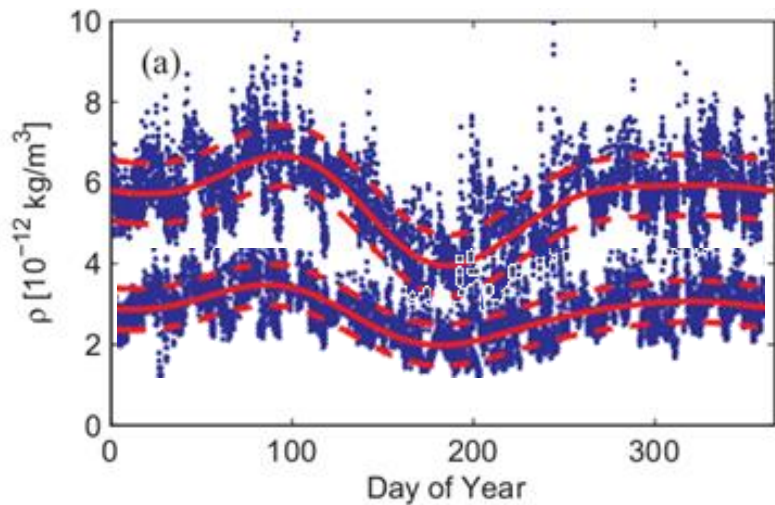
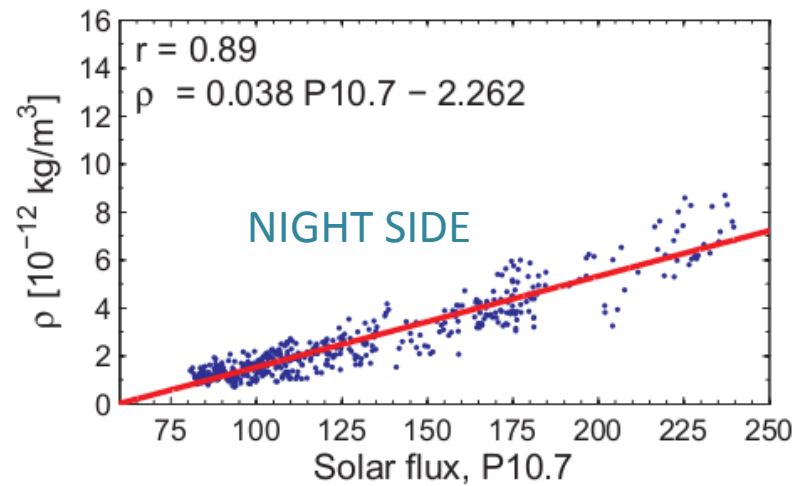
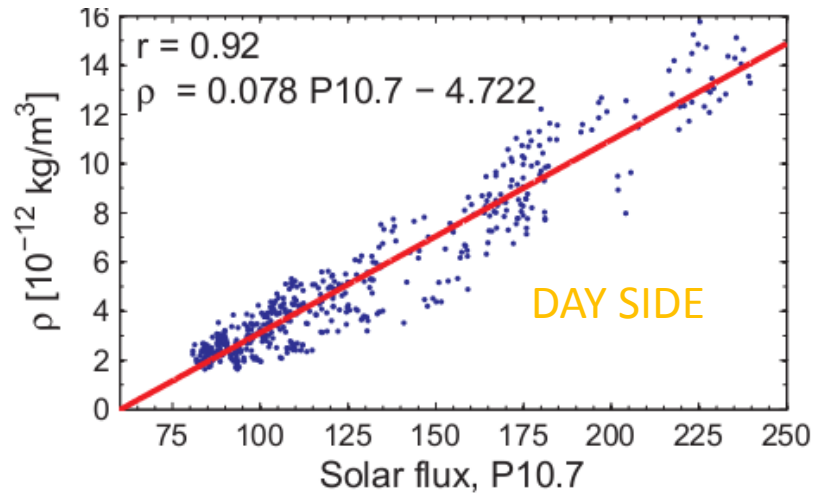
Equatorial mass anomaly (EMA)



*Liu et al. (2005, 2007 and 2009)

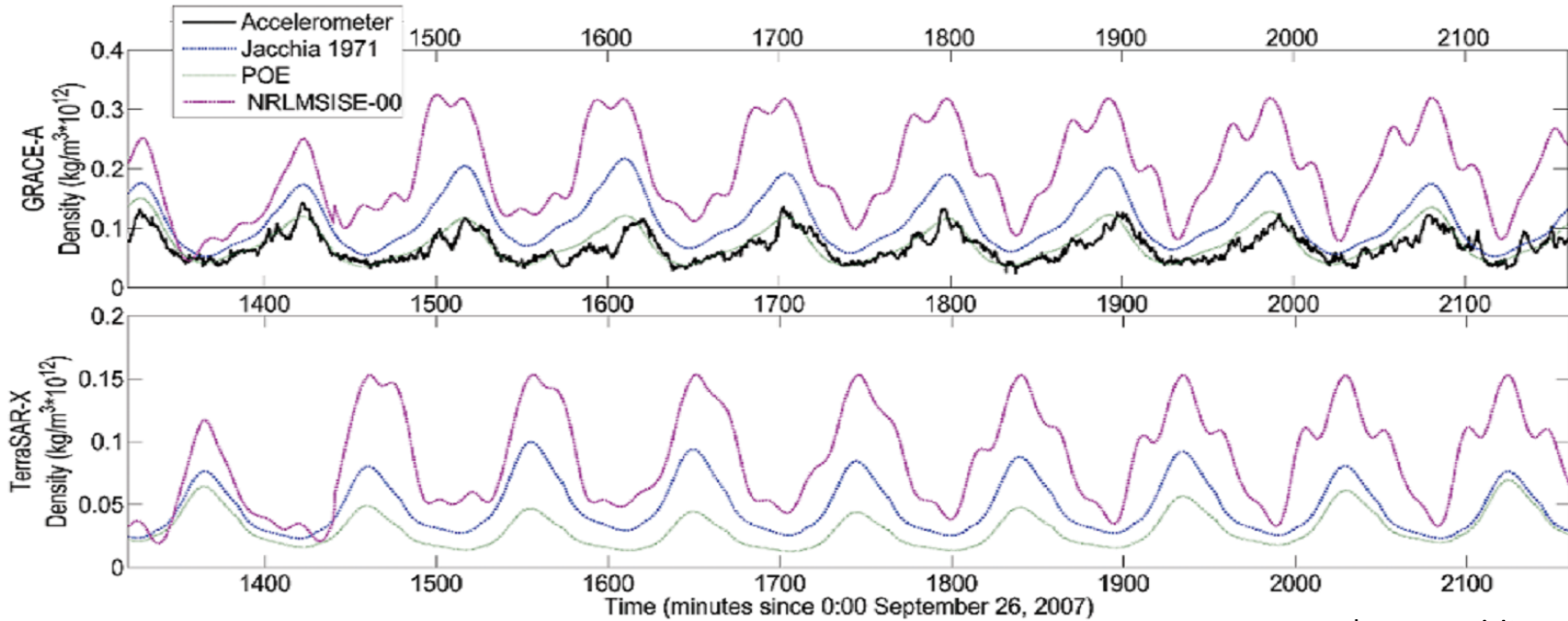
2. Progress, Problems & Motivation

Solar and magnetospheric forcing

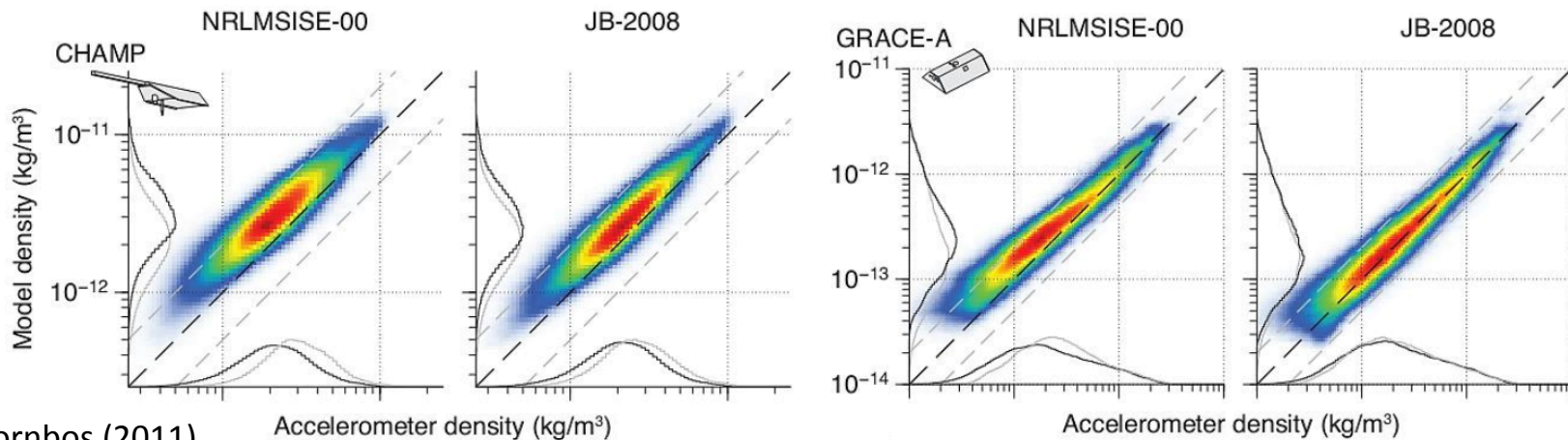


2. Progress, Problems & Motivation

Measurements & Empirical models



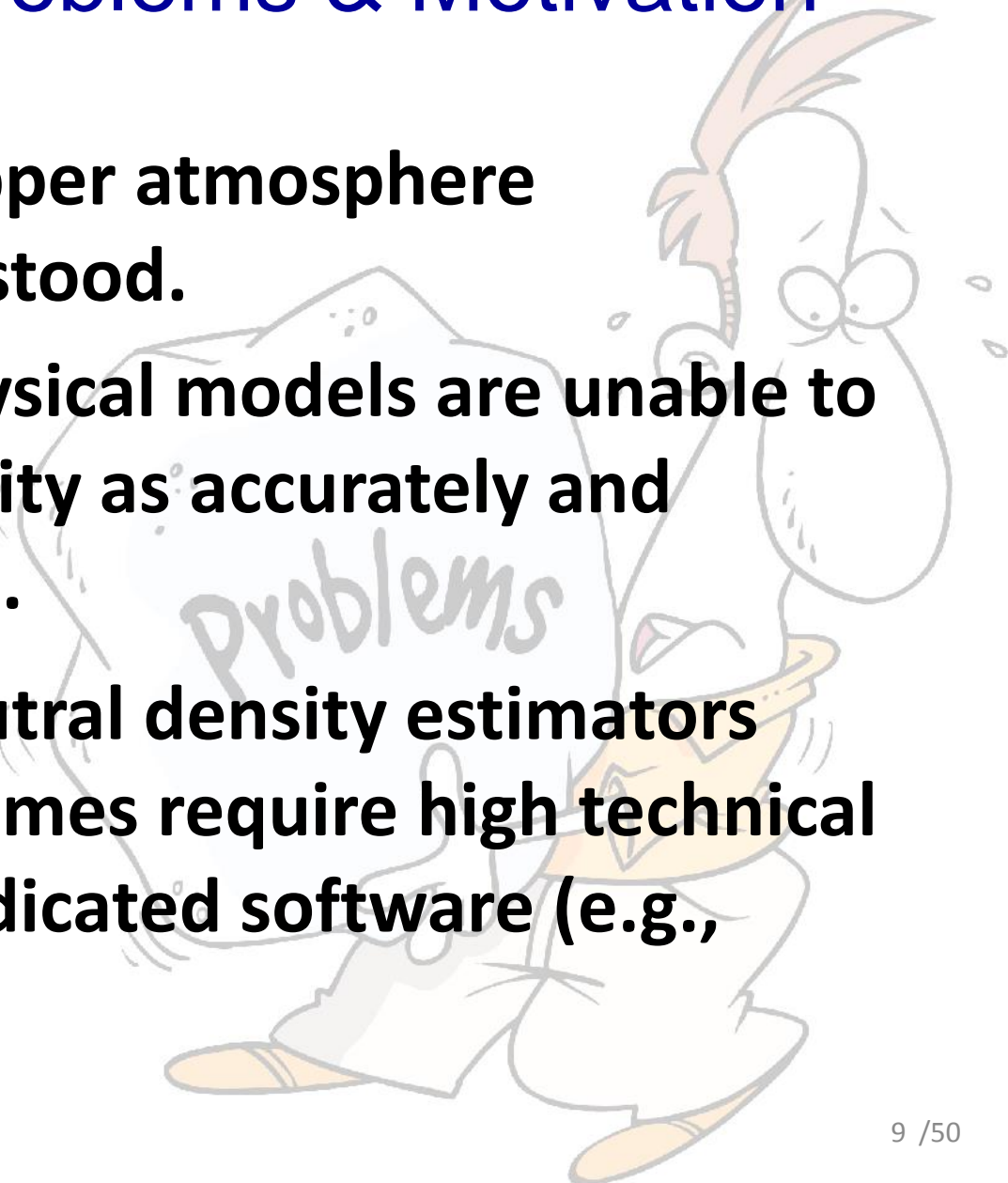
*McLaughlin et al. (2013)



*Doornbos (2011)

2. Progress, Problems & Motivation

- **Processes in the upper atmosphere are not well understood.**
- **The current geophysical models are unable to predict the variability as accurately and efficiently required.**
- **Thermospheric neutral density estimators based on POD schemes require high technical knowledge and dedicated software (e.g., GEODYN, ODTK).**

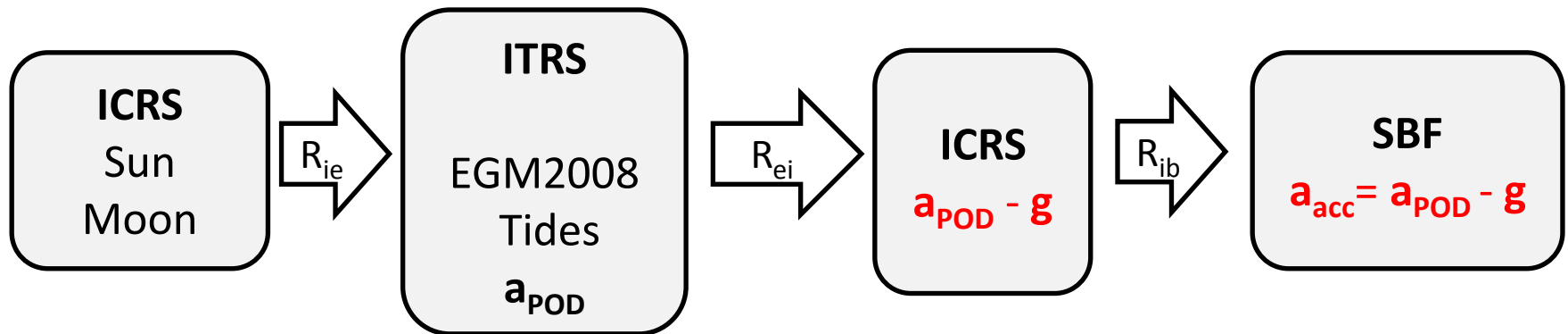


2. Progress, Problems & Motivation

- **A new technique based on numerical differentiation of POE is proposed for accelerometer calibration and density estimation.**
- **A new technique based in the PCA for the spatiotemporal analysis of satellite measurements along orbits is employed in 3 case-studies:**
 - 1. Conservative-force anomalies from analytical TVG, POE, and accelerometer measurements.**
 - 2. Differences between accelerometer-based densities and the NRLMSISE00 estimates (2003-2015).**
 - 3. Thermospheric neutral density distribution and variations from GRACE (2003-2015).**

3. Methods & Data processing

Reference systems for accelerometer calibration



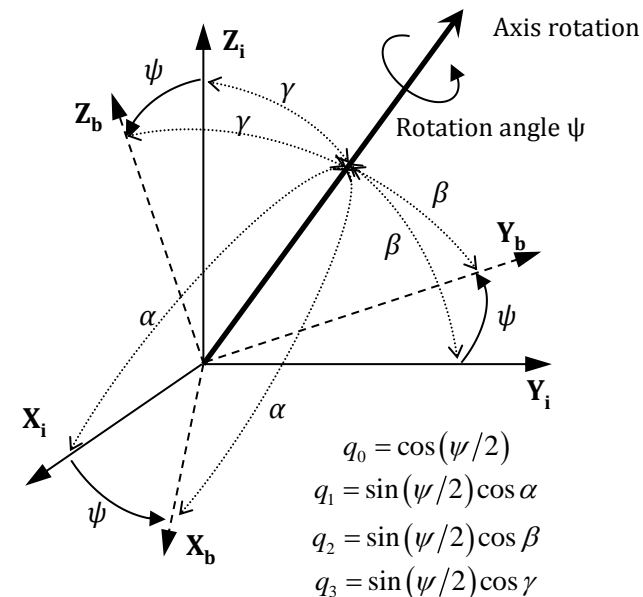
- R_{ei} rotation Earth-fixed to ICRS :

$$\mathbf{r}_{ICRS} = [P][N][S][PM]\dot{\mathbf{r}}_{ITRS}$$

$$\dot{\mathbf{r}}_{ICRS} = [P][N][S]\{[PM]\dot{\mathbf{r}}_{ITRS} + \boldsymbol{\omega}_{\oplus} \times [PM]\mathbf{r}_{ITRS}\}$$

- R_{ib} rotation ICRS to SBS by using star camera quaternion:

$$\mathbf{r}_{SBS} = [R_{ib}]\mathbf{r}_{ICRS} = \begin{bmatrix} q_0^2 + q_1^2 - q_2^2 - q_3^2 & 2(q_1q_2 + q_0q_3) & 2(q_1q_3 - q_0q_2) \\ 2(q_1q_2 - q_0q_3) & q_0^2 - q_1^2 + q_2^2 - q_3^2 & 2(q_2q_3 + q_0q_1) \\ 2(q_1q_3 + q_0q_2) & 2(q_2q_3 - q_0q_1) & q_0^2 - q_1^2 - q_2^2 + q_3^2 \end{bmatrix} \mathbf{r}_{ICRS}$$



3. Methods & Data processing

Drag force for density retrieval

- Drag-force formula:

$$F_D = ma_D = \frac{1}{2} CA\rho v_r^2$$

C Drag coefficient (Cook, 1965; Metha et. al, 2013)

A Cross-sectional area

ρ Atmospheric density

v_r Relative velocity of the atmosphere

m Satellite mass

a_D Aerodynamic acceleration

- Normalization to common altitude :

$$\rho(475km) = \rho_{obs}(h) \frac{\rho_{mod}(475km)}{\rho_{mod}(h)}$$

3. Methods & Data processing

POE-based non-gravitational accelerations

$$\mathbf{a}_{ng} = \mathbf{a}_{acc} = \mathbf{a}_{POE} - \mathbf{g}$$

- First derivatives of precise-orbit velocities are numerically differentiated under arc-to-chord interpolation-threshold

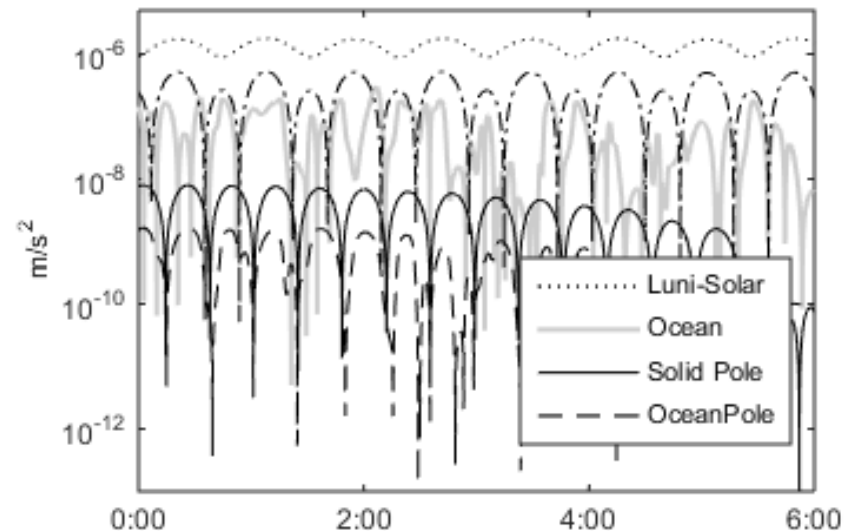
$$\ddot{\mathbf{r}}_{t_0} = \lim_{\Delta t \rightarrow 0} \dot{\mathbf{r}}''_{t_0} = \lim_{\Delta t \rightarrow 0} \frac{\dot{\mathbf{r}}'_{t_1} - \dot{\mathbf{r}}'_{t_{(-1)}}}{\Delta t} = \lim_{\Delta t \rightarrow 0} \frac{\mathbf{r}_{t_2} - 2\mathbf{r}_{t_0} + \mathbf{r}_{t_{(-2)}}}{(\Delta t)^2}$$

- Varying gravity field model (\mathbf{g})

- Conventional model EGM2008.
- Secular low degree C_{20} (zero-tide),
- C_{30} and C_{40} rates.
- C_{21} and S_{21} mean pole coefficients.
- Third body direct tides (Luni-solar).
- Solid Earth tides.
- Ocean tides (EOT11a).
- Solid Earth pole tide.
- Ocean pole tide.
- Schwarzschild terms for relativity.

Interpolation threshold
And corresponding error

Δt (s)	Error (nm/s ²)
0.05	1
0.1	3
0.2	12
0.5	50
1	120
2	1500



*Calabia and Jin (2015)

3. Methods & Data processing

Aerodynamic acceleration

Radiation-pressure removal:

Solar radiation

$$a_{sr} = \sum_{i=1}^{n_p} - \frac{E_{sr} A_i \hat{n}_i \hat{S}_{Sun}^{sat}}{mc} \left[2 \left(\frac{c_{rd,i}}{3} + c_{rs,i} \hat{n}_i \hat{S}_{Sun}^{sat} \right) \hat{n}_i + (1 - c_{rs,i}) \hat{S}_{Sun}^{sat} \right]$$

Earth albedo

$$a_{ea} = \sum_{i=1}^{n_p} \sum_{j=1}^{grid} - \frac{E_{ea,j} A_i \hat{n}_i \hat{S}_j^{sat}}{mc} \left[2 \left(\frac{c_{rd,i}}{3} + c_{rs,i} \hat{n}_i \hat{S}_j^{sat} \right) \hat{n}_i + (1 - c_{rs,i}) \hat{S}_j^{sat} \right]$$

$$E_{ea,j} = E_{ea}^R + E_{ea}^{IR}$$

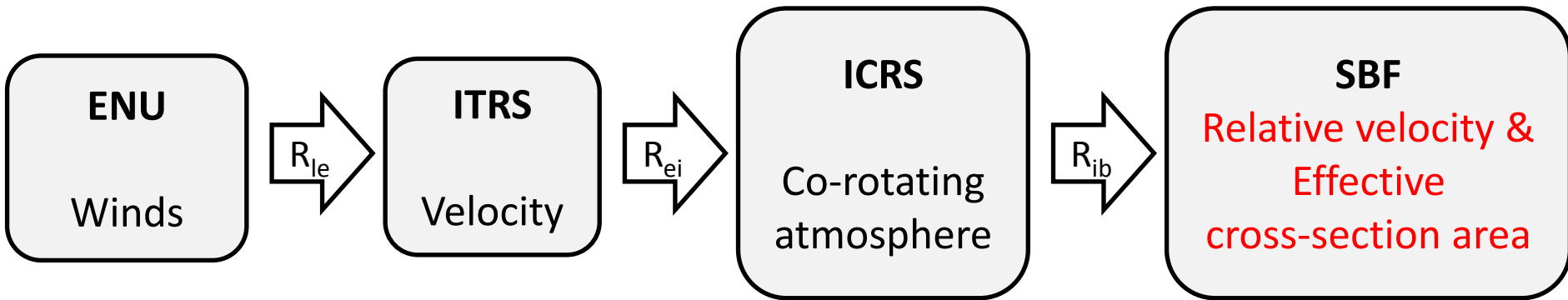
$$E_{ea,j}^R = f_j v_j E_{sr} \frac{A_j (\hat{n}_j \hat{S}_j^{Sun}) (\hat{n}_j \hat{S}_j^{sat}) \sigma_{TOMS}}{\pi |\hat{S}_j^{sat}|^2}$$

$$E_{ea,j}^{IR} = f_j 239 \left(\frac{1AU}{S_{Sun}^j} \right)^2 e_{IR,j} \frac{A_j \hat{n}_j \hat{S}_j^{sat}}{\pi |\hat{S}_j^{sat}|^2}$$

$$a_D = a_{ng} - a_{sr} - a_{ea}$$

3. Methods & Data processing

Reference systems in density retrieval



R_{ei} rotation Earth-fixed to ICRS :

$$\dot{\mathbf{r}}_{ICRS} = [PREC][NUT][ST] \{ [PM] \dot{\mathbf{r}}_{ITRS} + \boldsymbol{\omega}_{\oplus} \times \mathbf{r}_{ITRS} \}$$

R_{ib} rotation ICRS to SBS by using star camera quaternion.

Relative velocity of the atmosphere with respect to the spacecraft

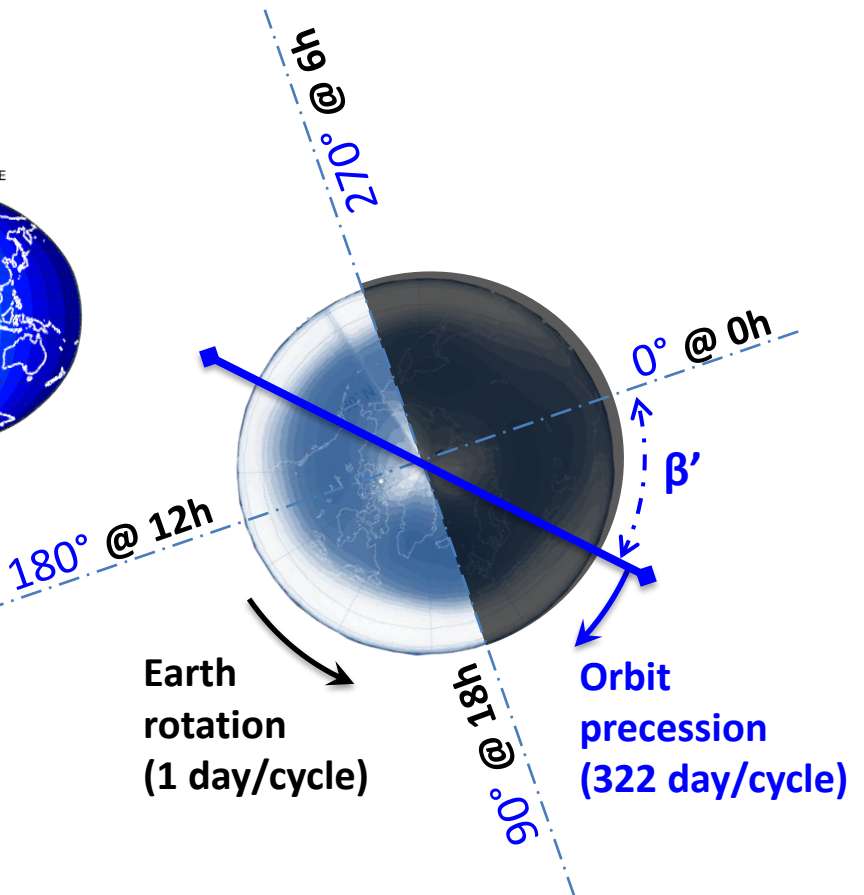
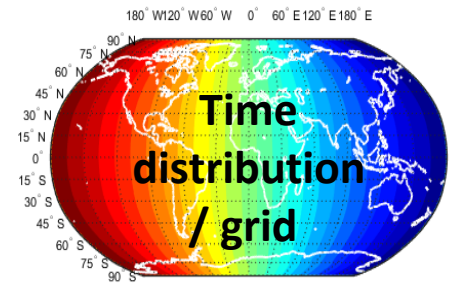
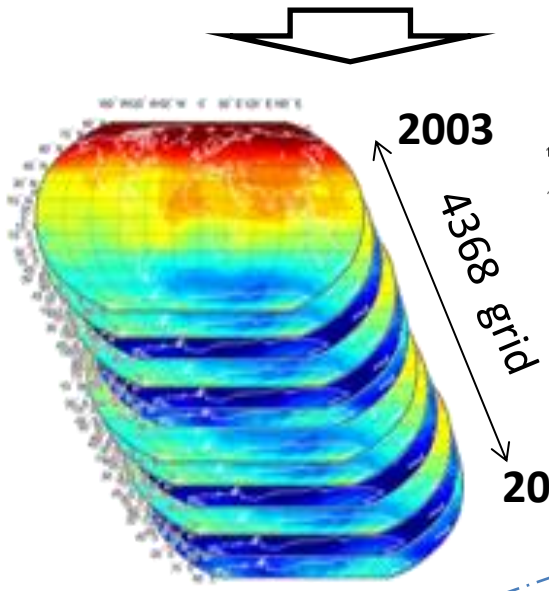
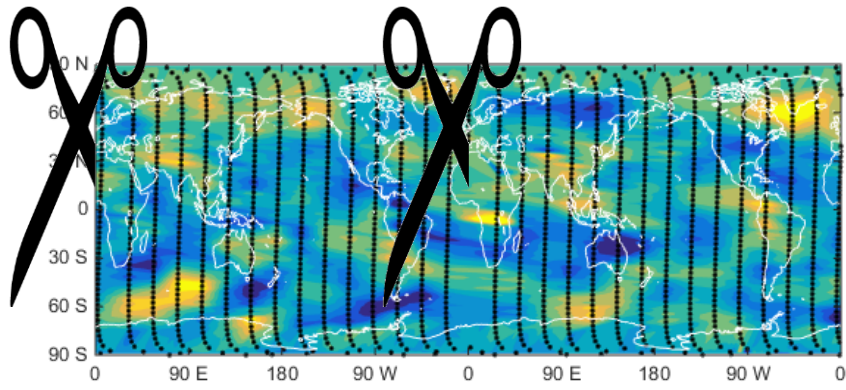
$$\mathbf{v}_r = -\dot{\mathbf{r}} + \mathbf{v}_{r,c} + \mathbf{v}_{r,w}$$

Horizontal winds from HWM07 and the co-rotating atmosphere:

$$\mathbf{v}_{r,c} = \boldsymbol{\omega}_{\oplus} \times \mathbf{r} = R_{ei}[0, 0, 0.7292115 \cdot 10^{-4} \text{sec}]^T \times \mathbf{r}$$

3. Methods & Data processing

- 1st Density along orbit
- 2nd Data interpolation
- 3rd Grid clipping

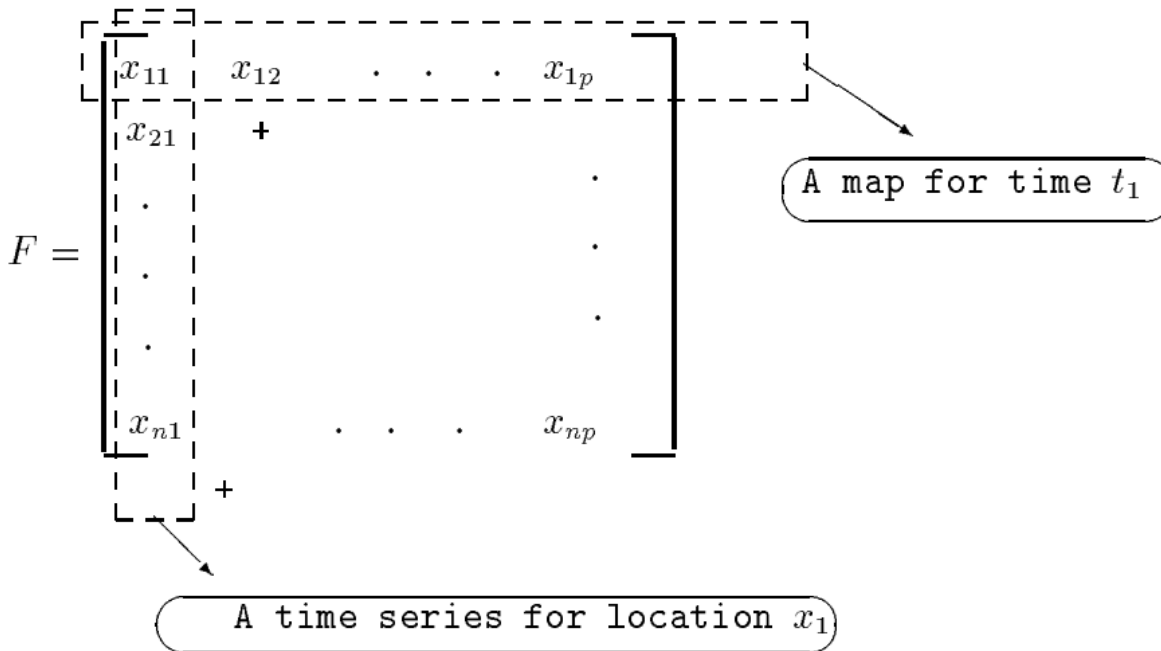


Annual variation (365 day)

3. Methods & Data processing

Principal Component Analysis (PCA)

4th Arrange each grid in a column.



5th Find the covariance matrix.

6th Find eigenvalues (time-coefficients) & eigenvectors (maps).

3. Methods & Data processing

Parameterization of time-expansion coefficients

7th Normalization to common flux (Muller et al. 2009):

$$\rho(P10.7 = 110) = \rho \frac{Fa(P10.7 = 110)}{Fa(P10.7)}$$

8th Fourier least-squares fitting:

$$\sum_{i=1}^n [a_n \cdot \cos(n \cdot \chi \cdot w) + b_n \cdot \sin(n \cdot \chi \cdot w)]$$

9th Polynomial fitting modulates the amplitude of the sinusoidal function computed in previous step:

$$G(\chi, P107) = 10^{-15} \cdot 10^a \cdot P107^b \cdot \left(a_0 + \sum_{i=1}^n [a_n \cdot \cos(n \cdot \chi \cdot w) + b_n \cdot \sin(n \cdot \chi \cdot w)] \right)$$

* a, b, a₀, a_n, b_n and w are the constant and amplitudes, and $\chi = (\text{doy}, \beta')$.

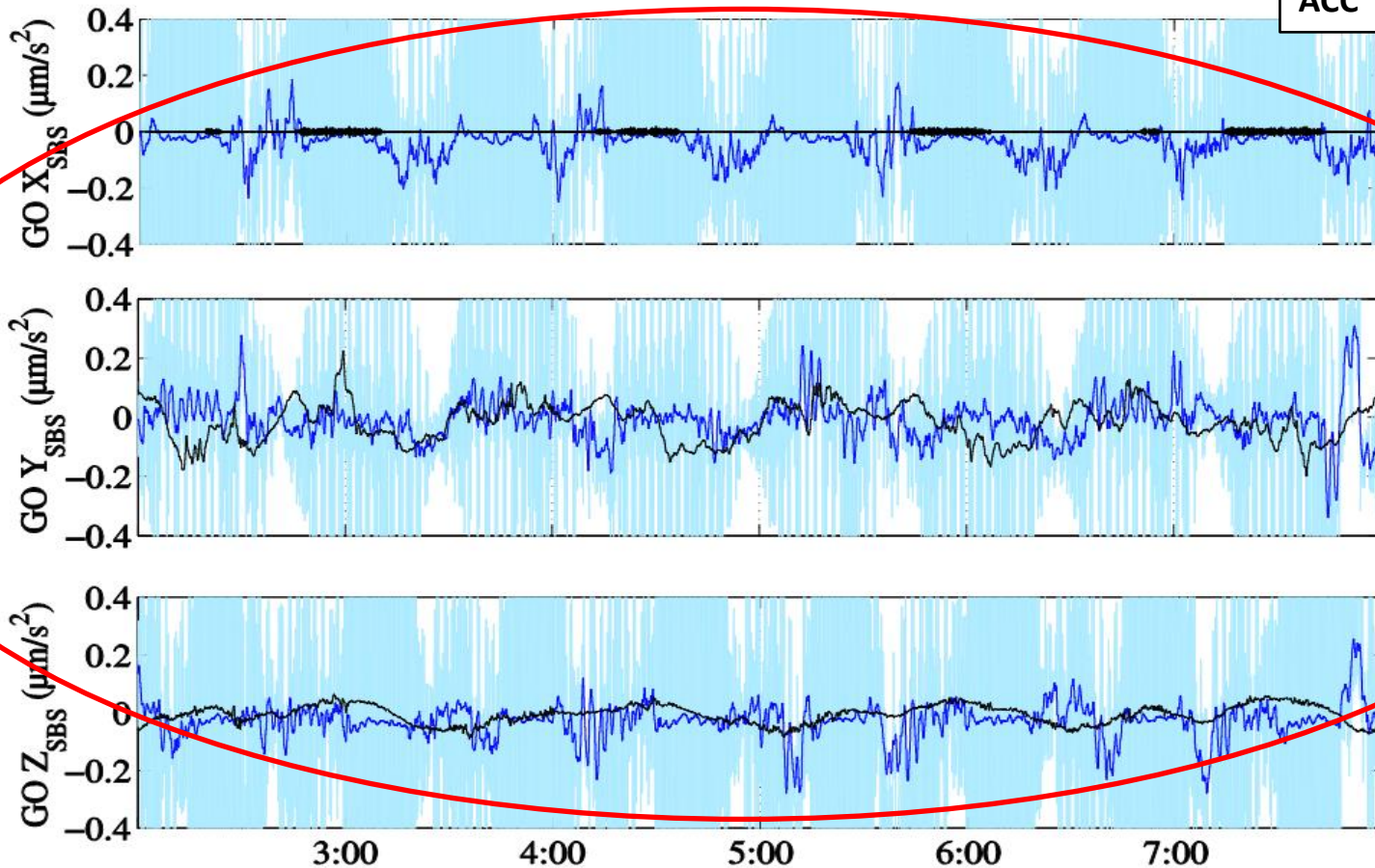
4.1. Results: POE vs ACC

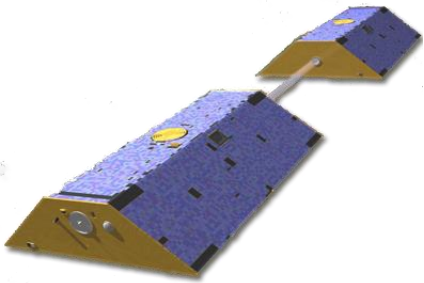
Smoothing and error removal

GOCE

POD ERRORS IN ALL THREE AXES

raw POE
smoothed POE
ACC



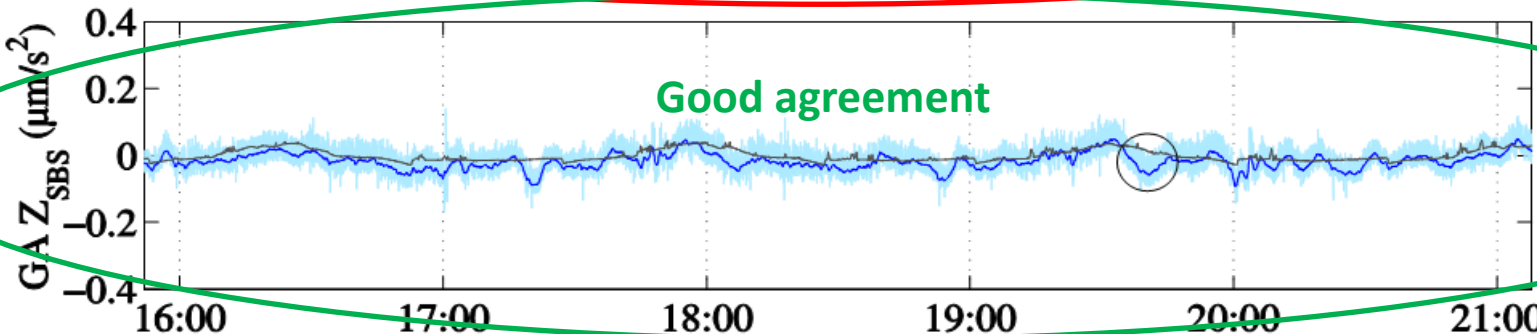
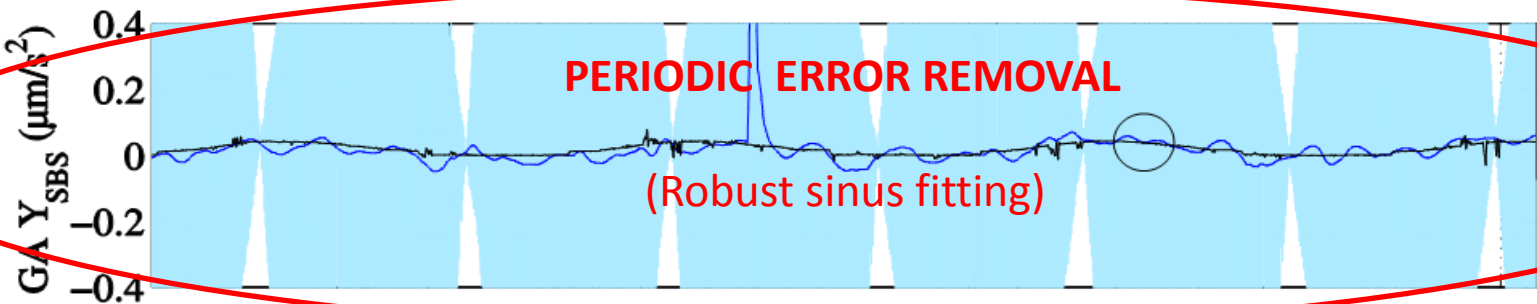
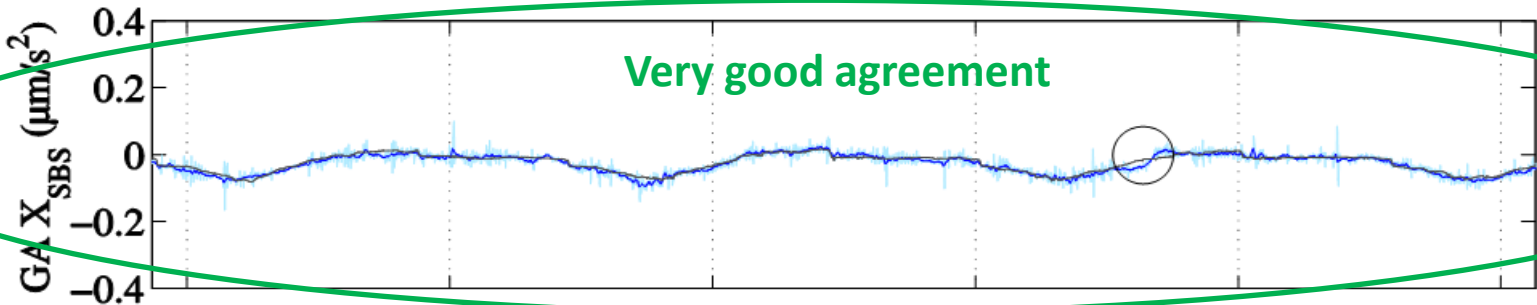


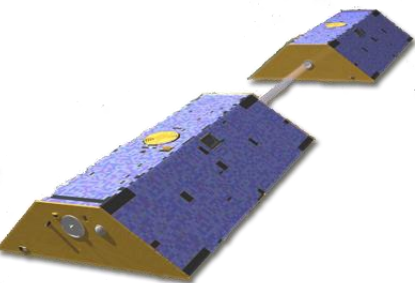
4.1. Results: POE vs ACC

Smoothing and error removal

GRACE

raw POE
smoothed POE
ACC

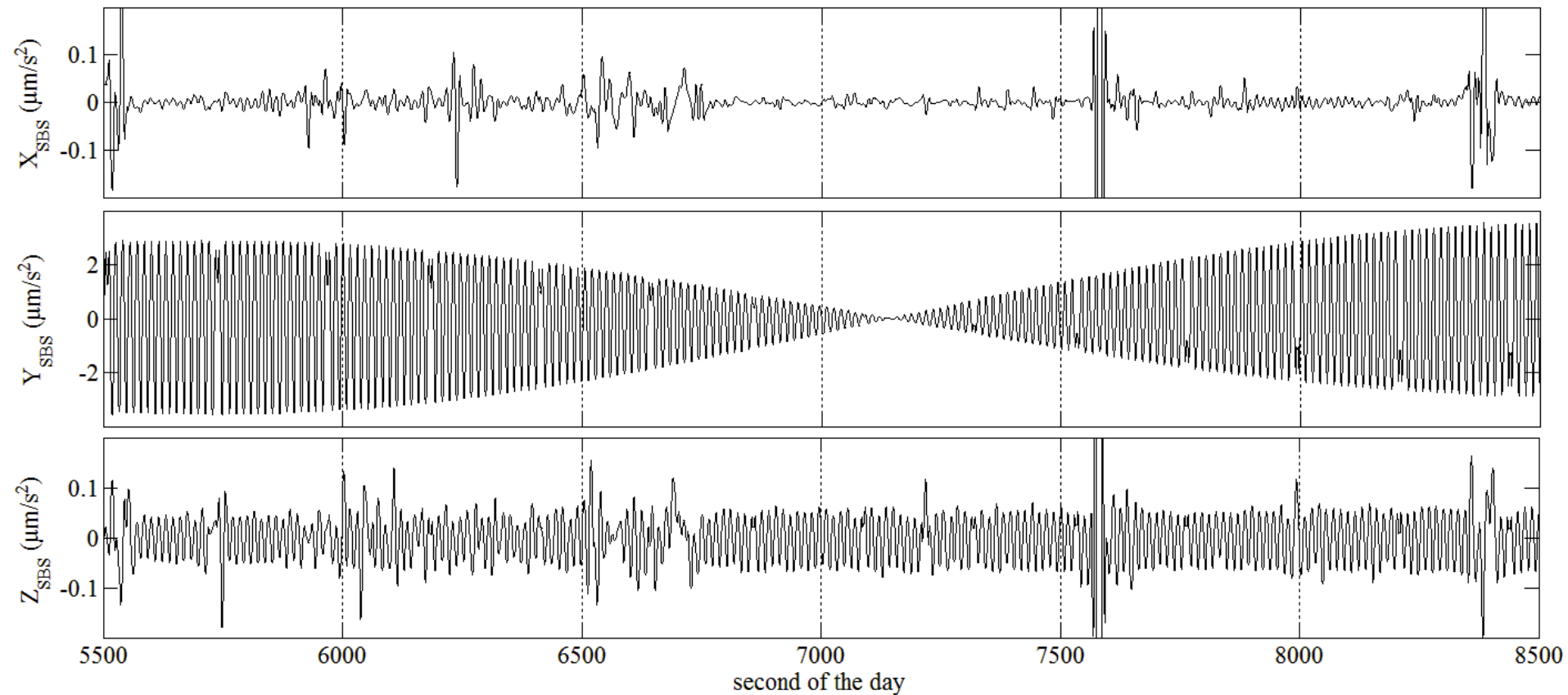




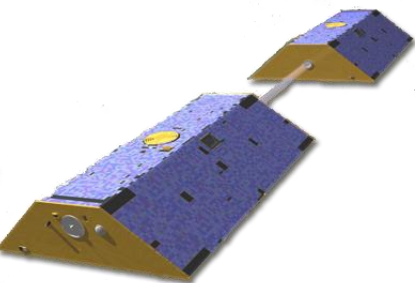
4.1. Results: POE vs ACC

Assessment of POD and force models

GRACE



Residuals after smoothing the solution and removing the systematic error on axis Y_{SBS}



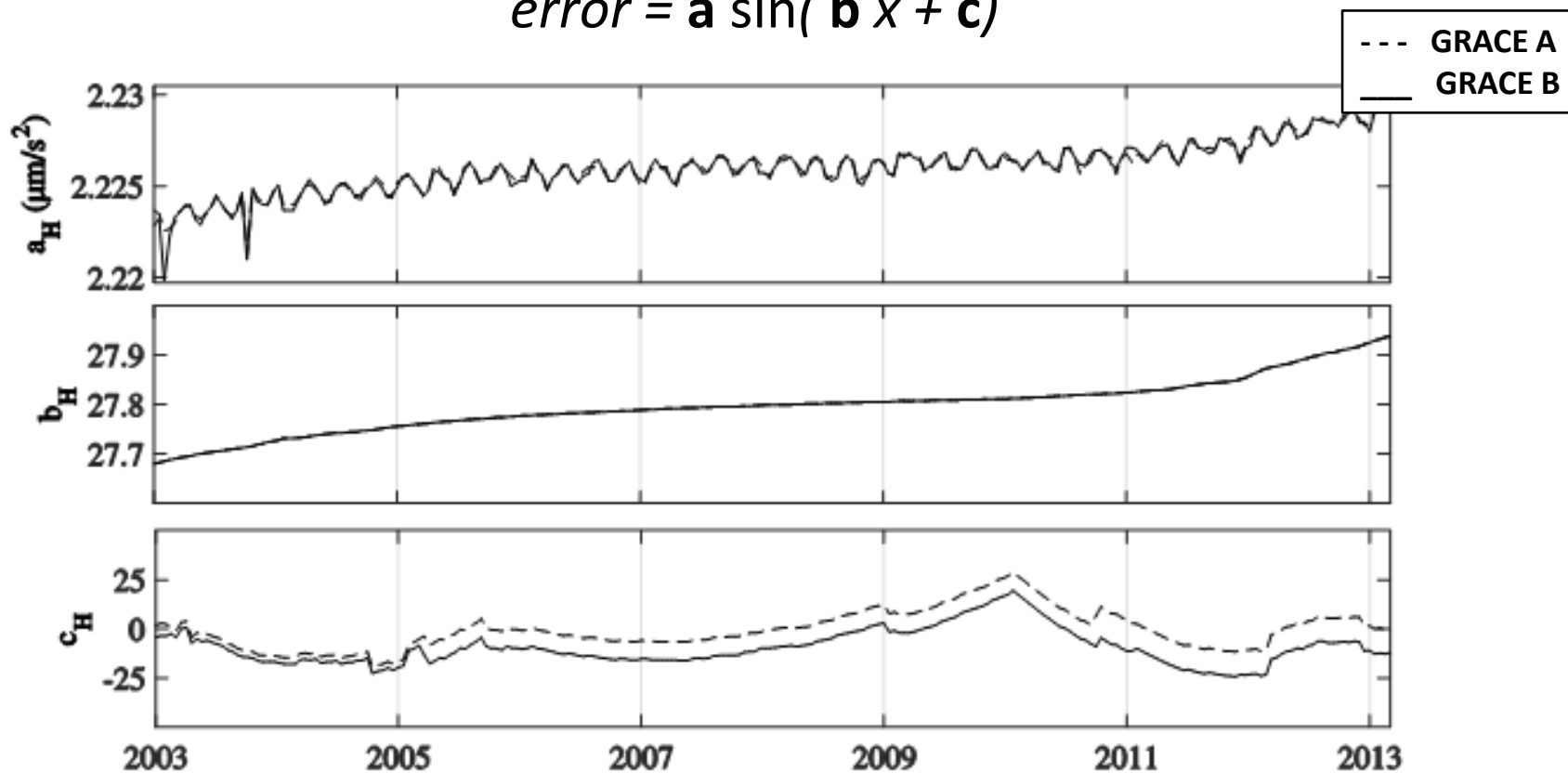
4.1. Results: POE vs ACC

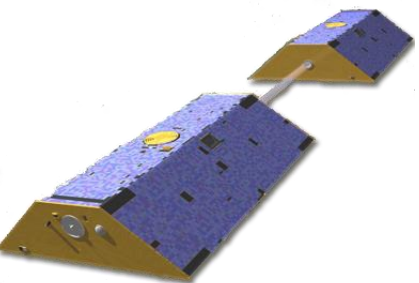
Assessment of POD and force models

GRACE

Fitted parameters for Y_{SBS} error:

$$\text{error} = \mathbf{a} \sin(\mathbf{b} x + \mathbf{c})$$

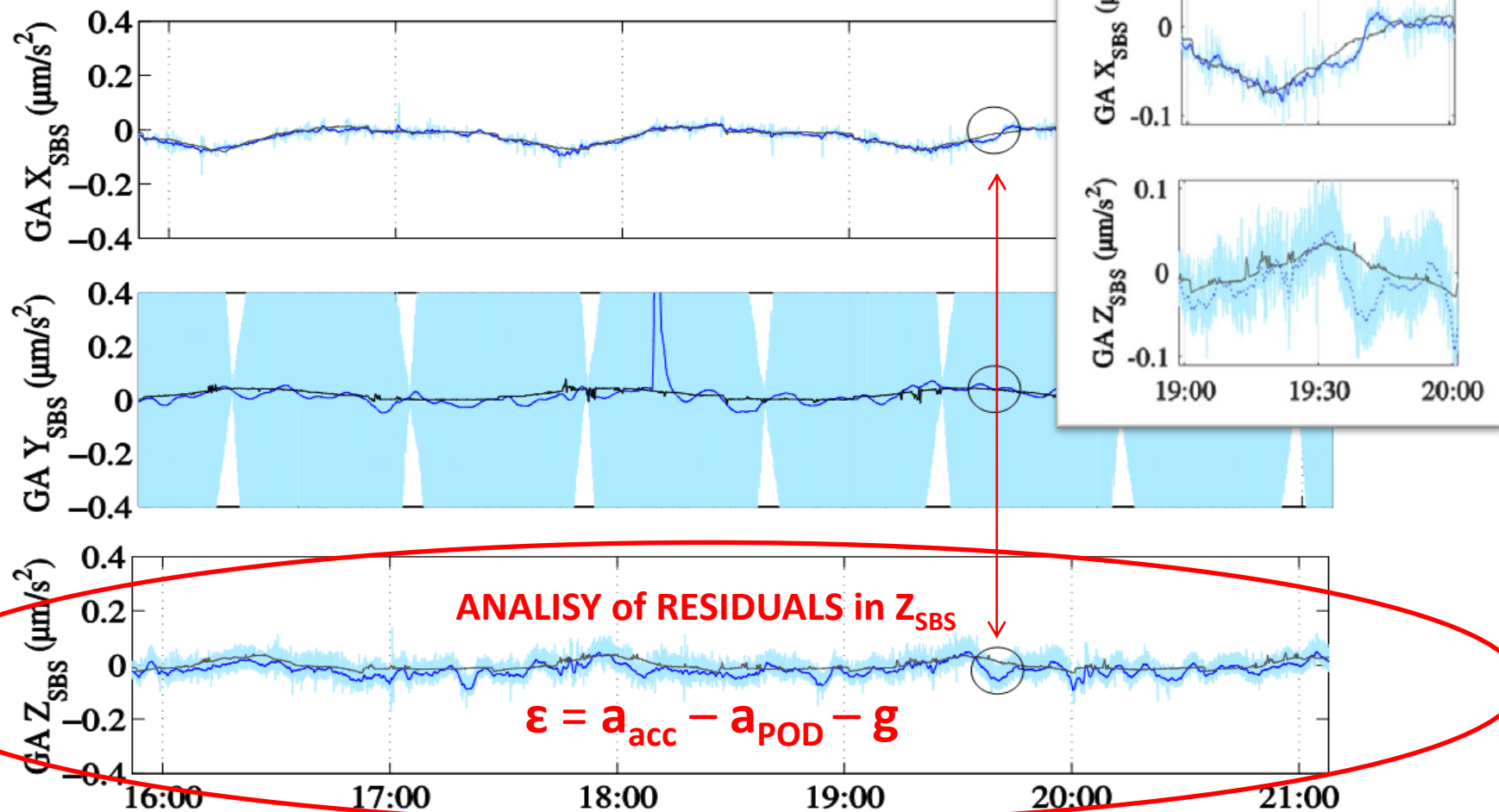




4.1. Results: POE vs ACC

Assessment of POD and force models

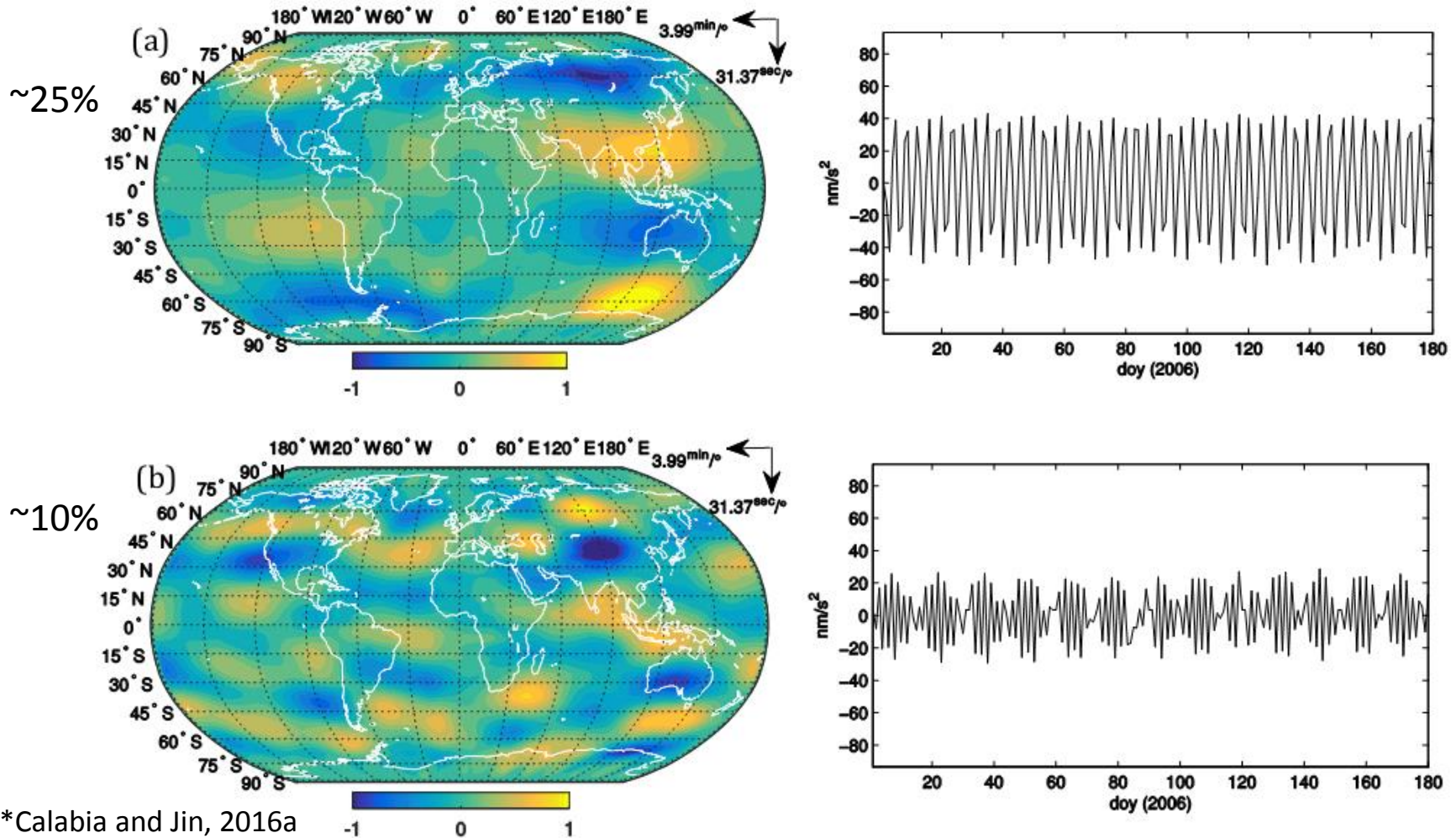
GRACE



4.1. Results: POE vs ACC

Assessment of POD and force models with PCA

Structures at the sub-daily frequency probably related to atmospheric tides.

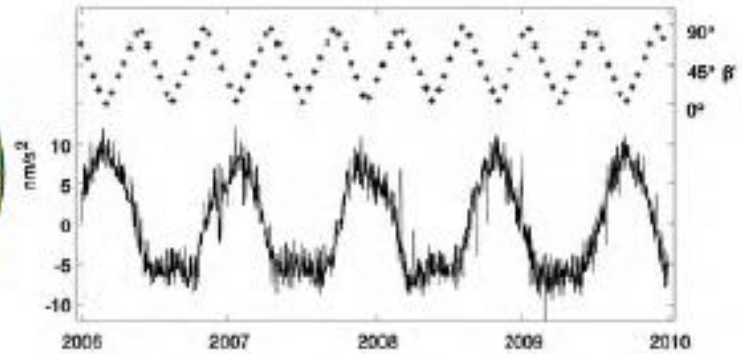
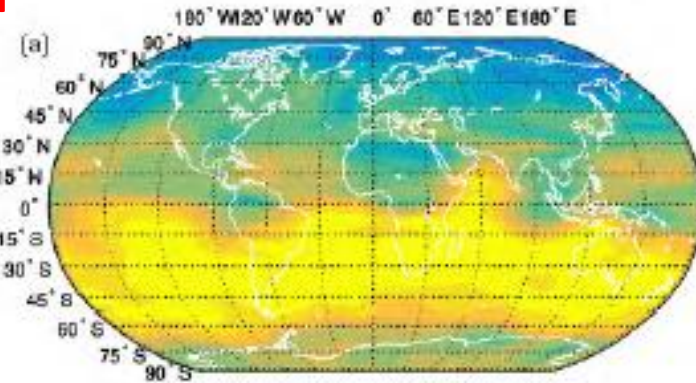


4.1. Results: POE vs ACC

Assessment of POD and force models with PCA

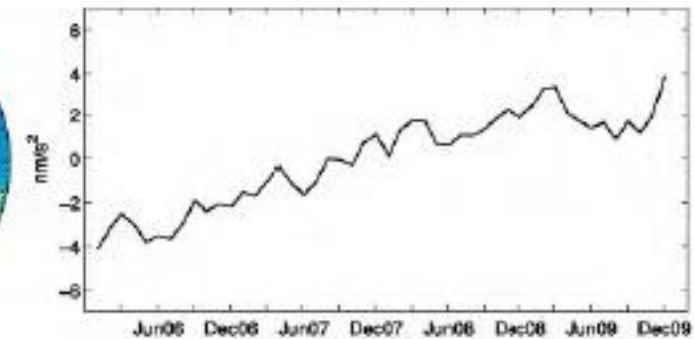
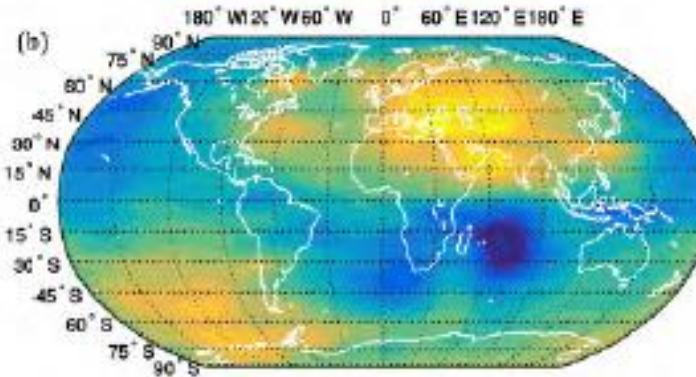
Latitudinal
variation

~5%

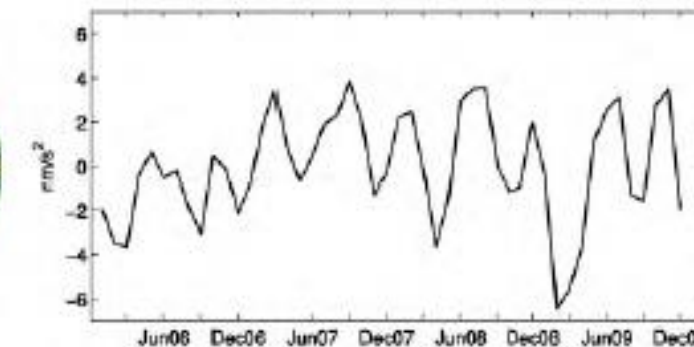
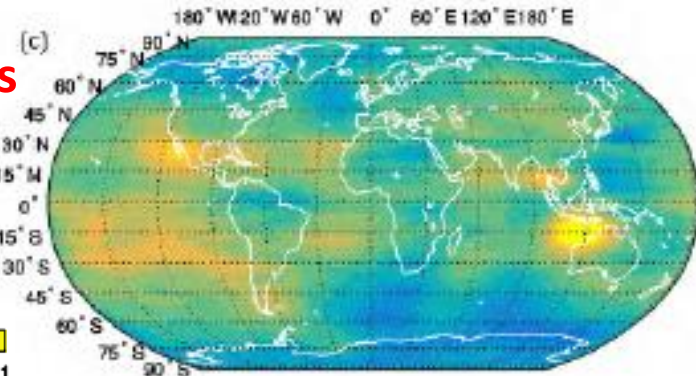


null at
 $\beta' = \pm 90^\circ$

Trend



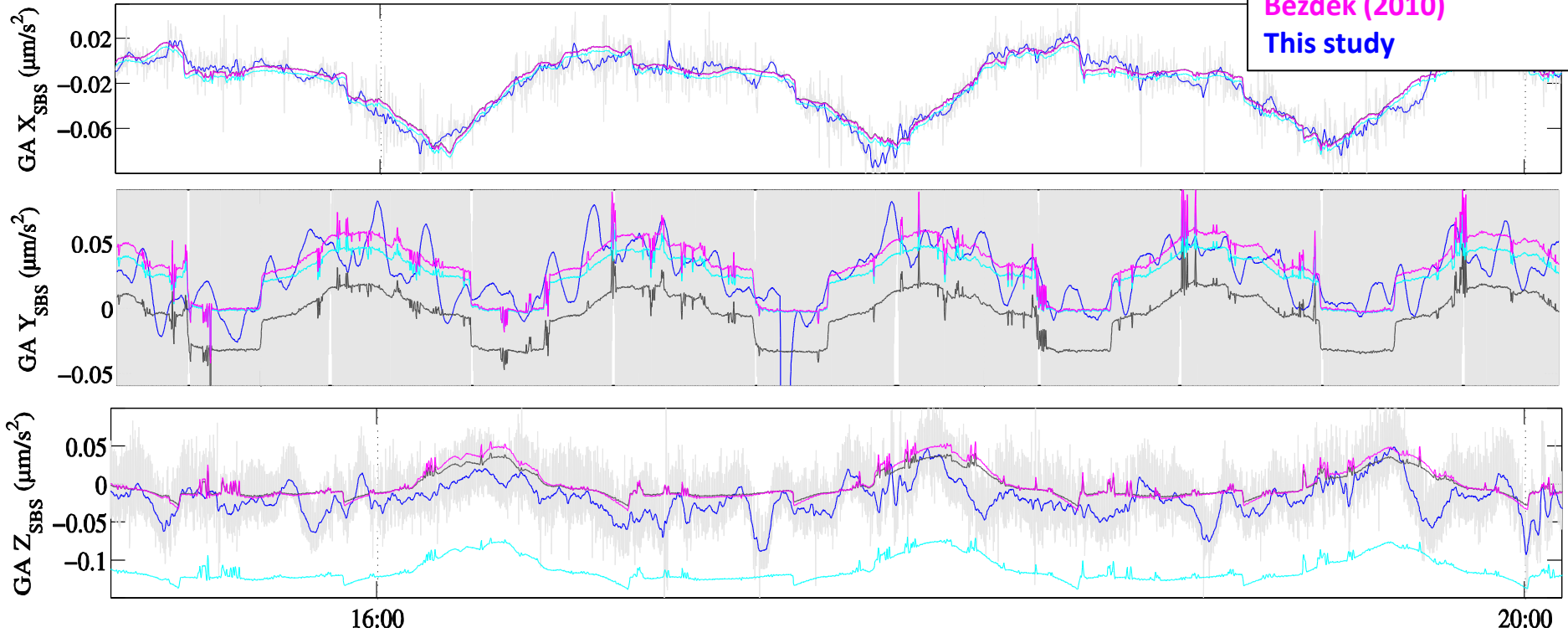
Local
variations



4.1. Results: POE vs ACC

Accelerometer calibration

Bettadpur (2009)
Bruinsma et al. (2007)
Bezdek (2010)
This study

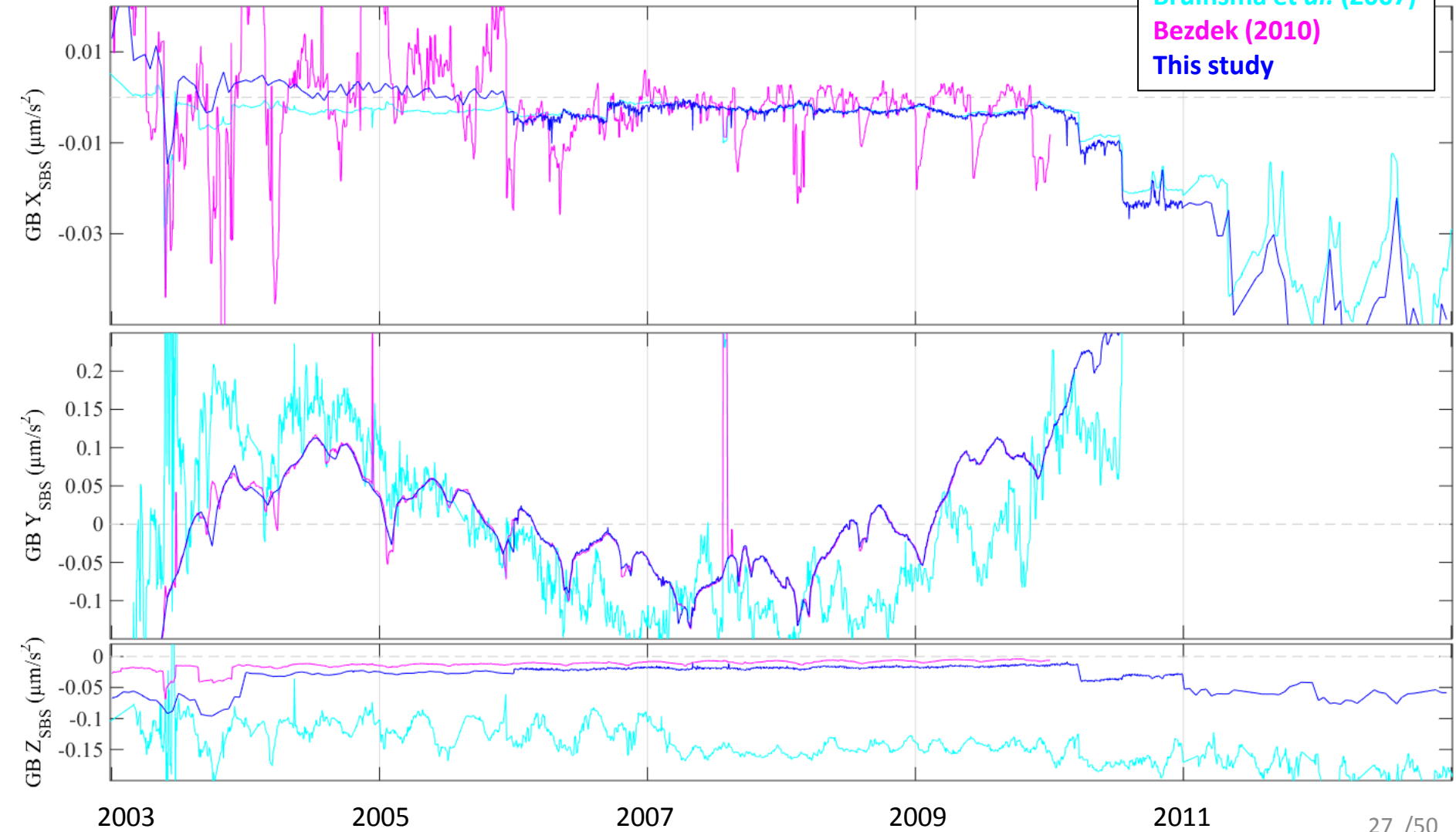


July 15th 2006

4.1. Results: POE vs ACC

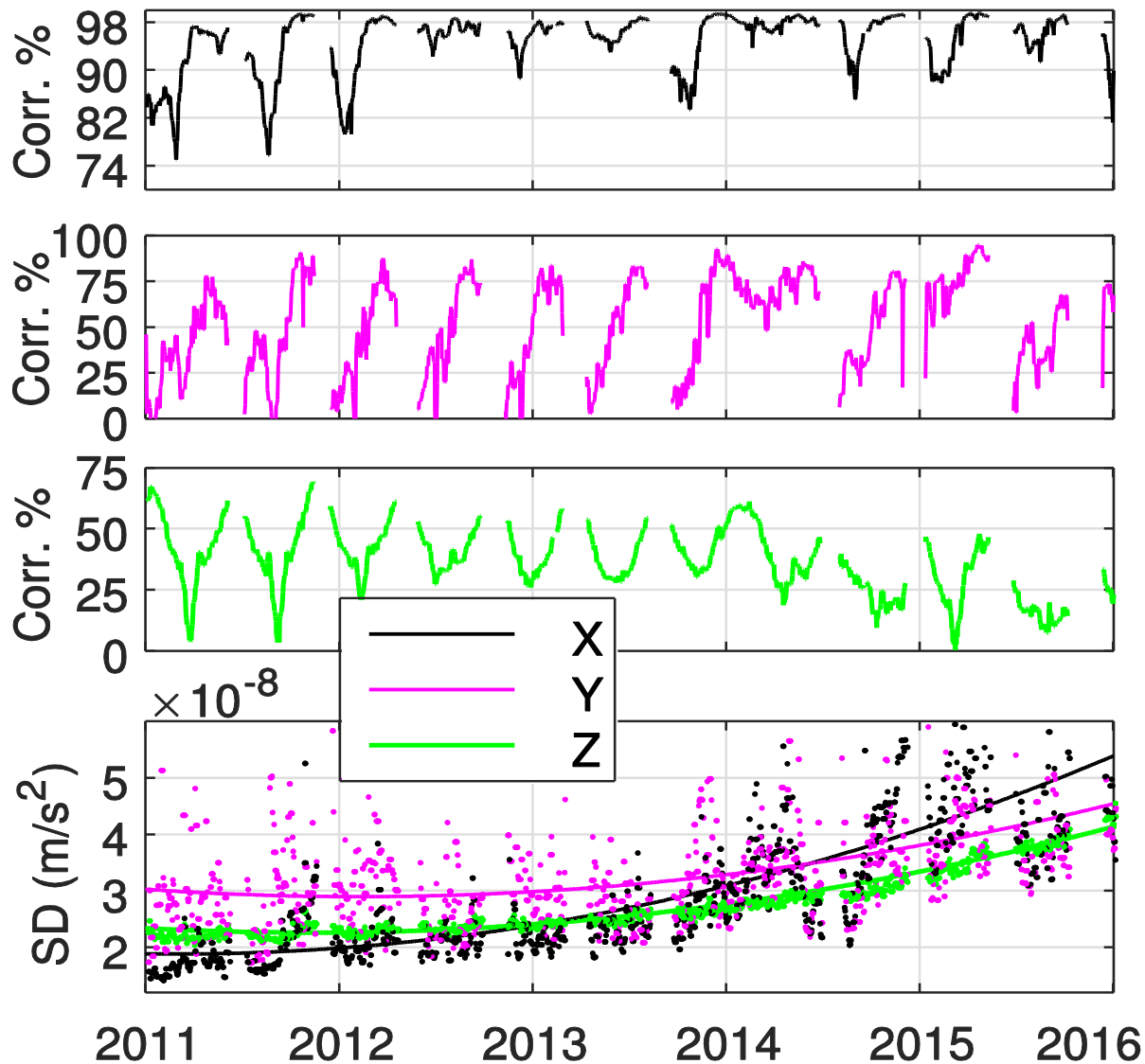
Accelerometer calibration

Bettadpur (2009)
Bruinsma et al. (2007)
Bezdek (2010)
This study



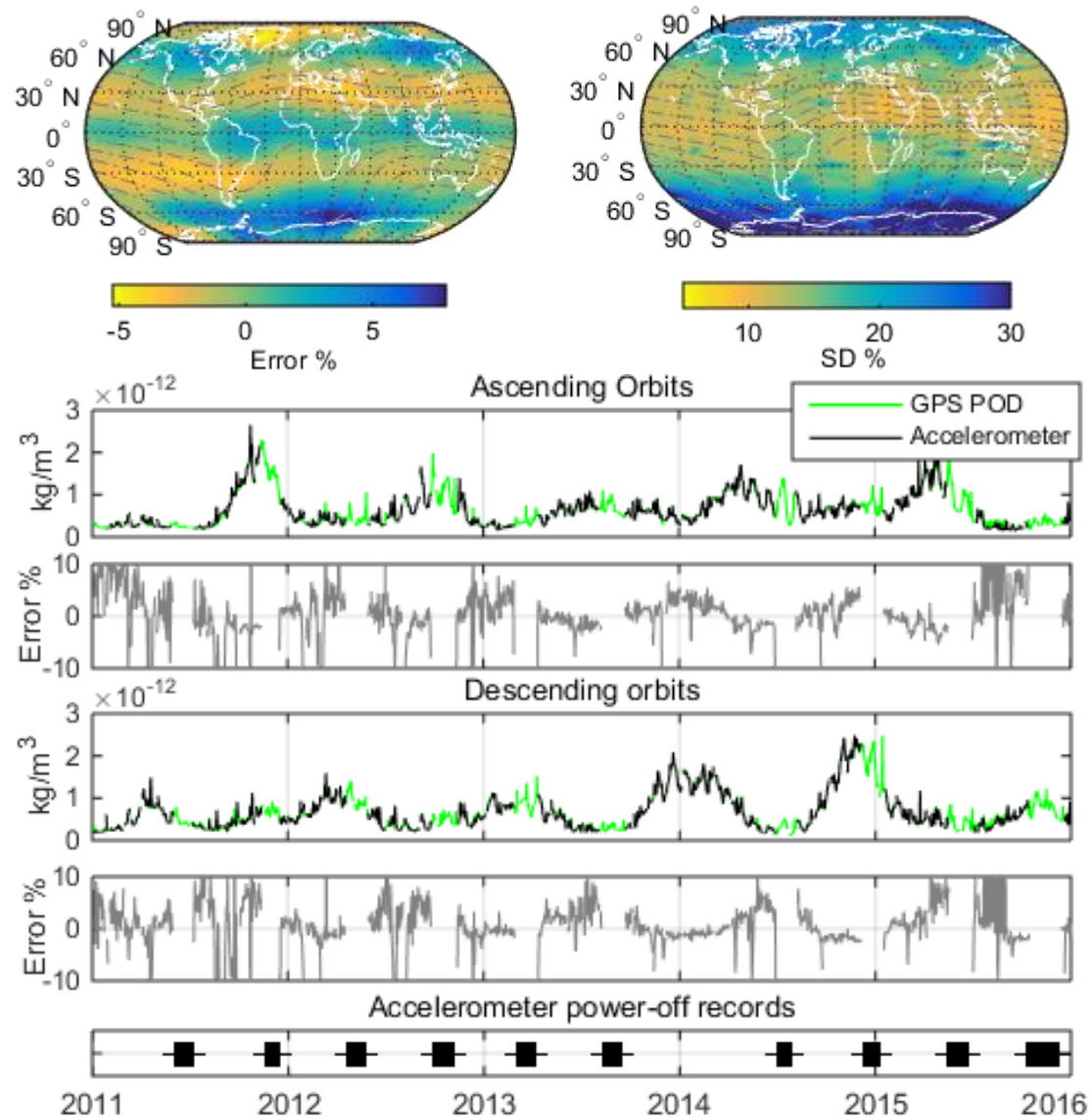
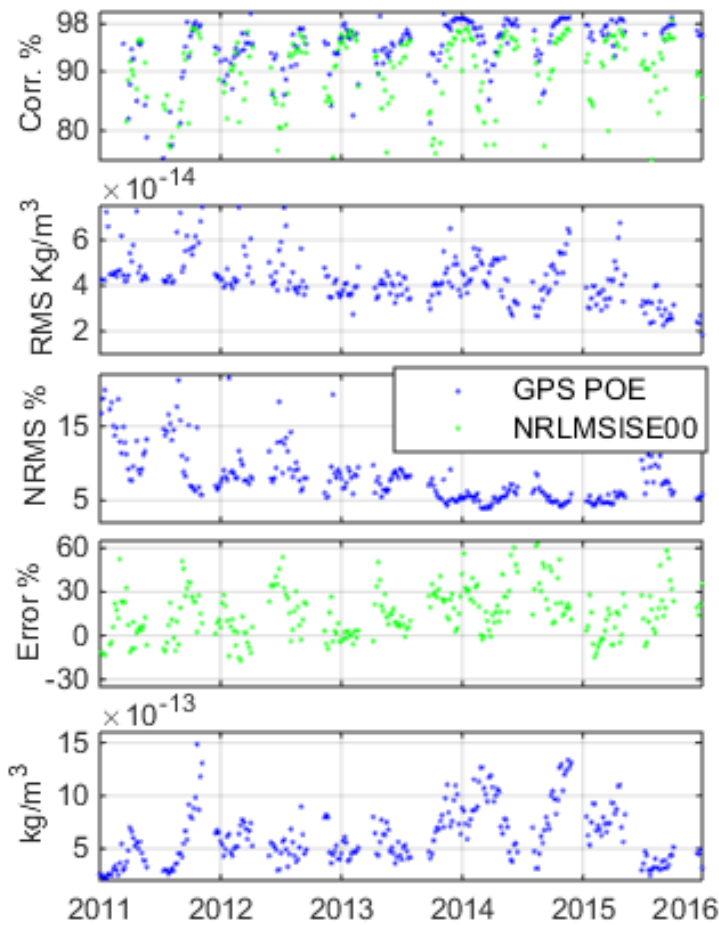
4.1. Results: POE vs ACC

Uncertainty of POE-based non-gravitational accelerations



4.1. Results: POE vs ACC

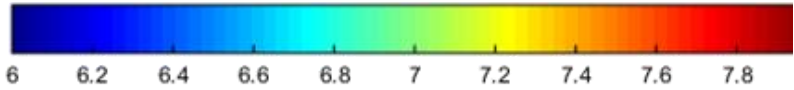
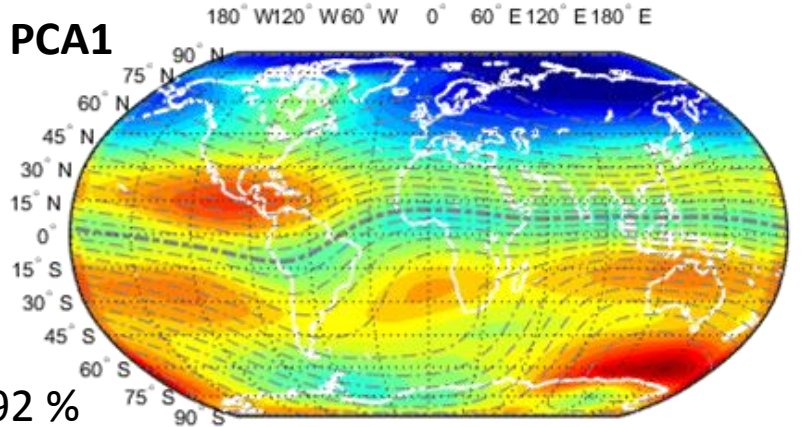
Uncertainty of new density estimates



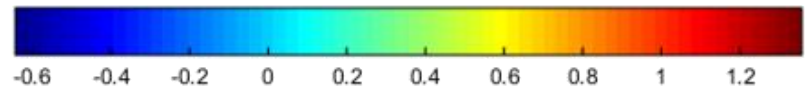
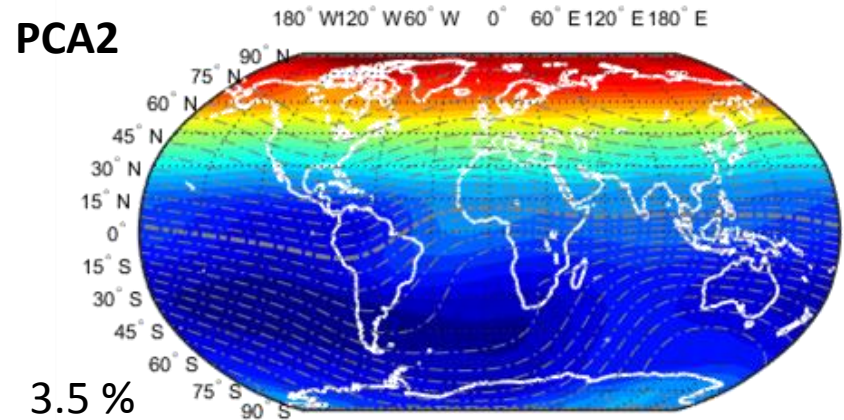
4.2. Results: PCA parameterization

Main PCA: **98.5%** variability

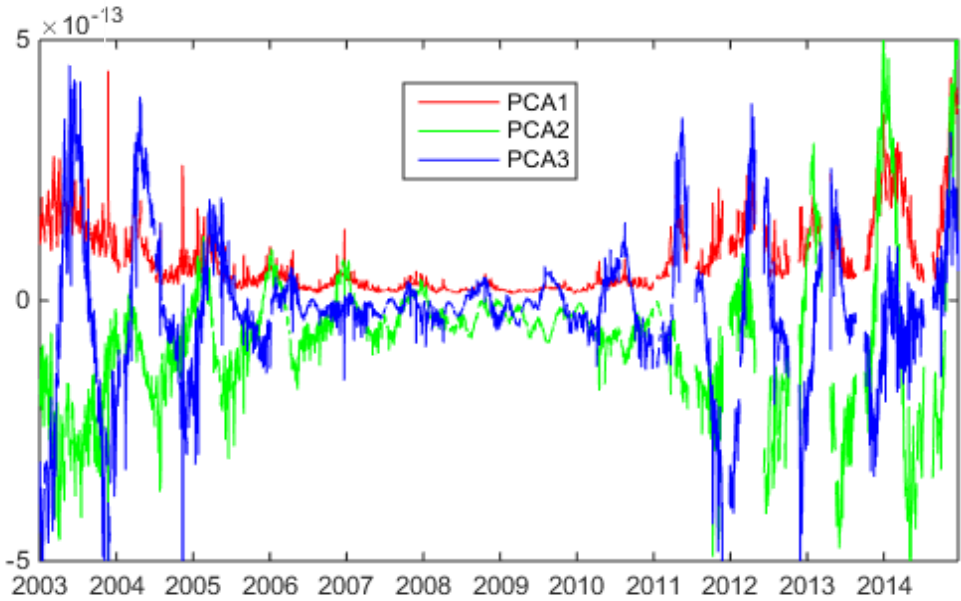
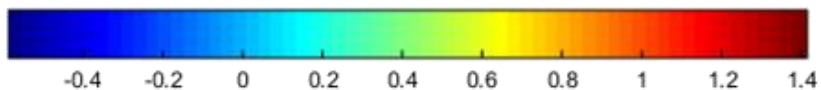
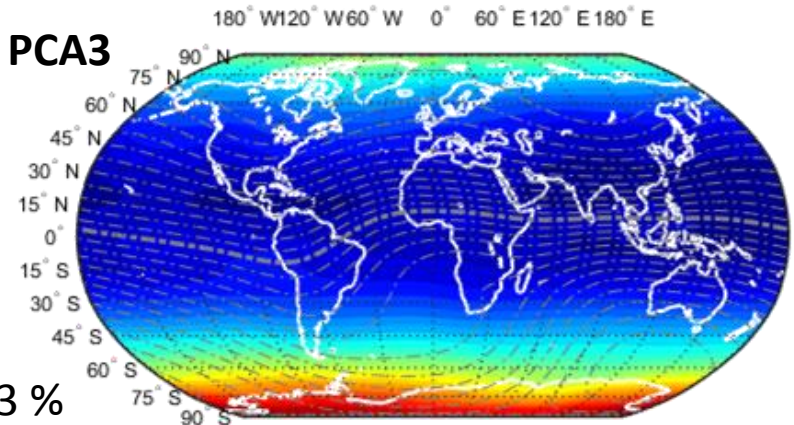
PCA1



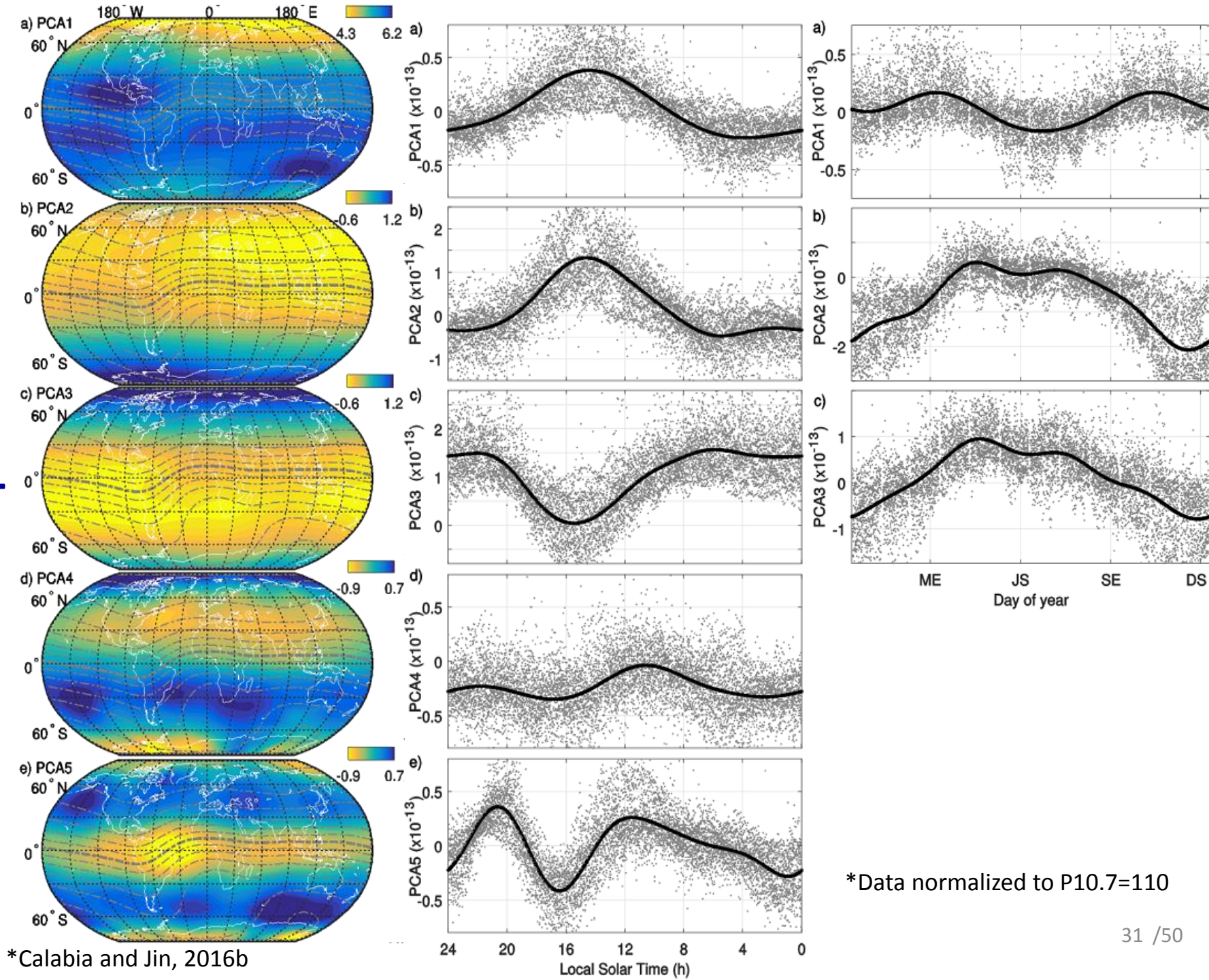
PCA2



PCA3



4.2. Results: PCA parameterization

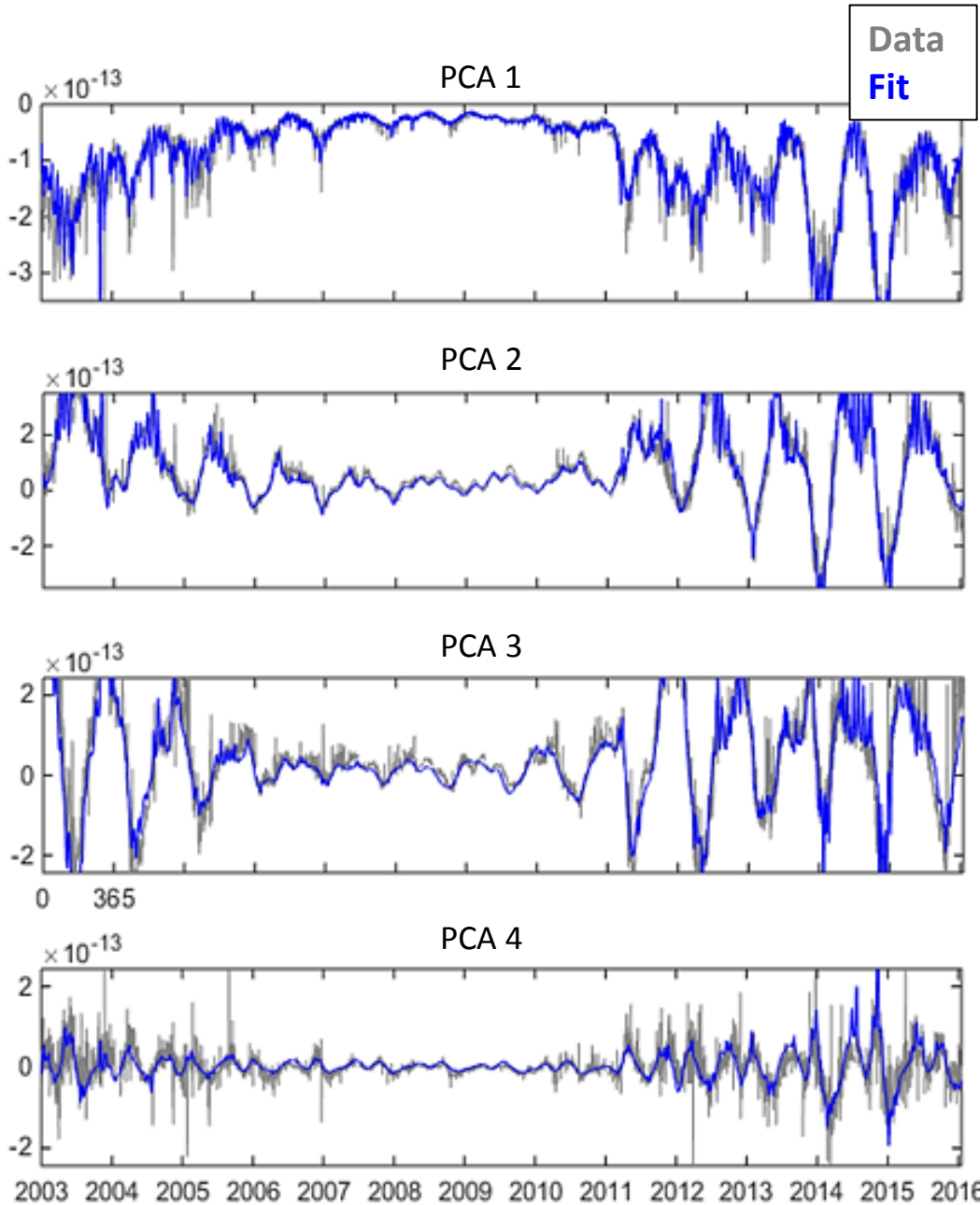


*Calabia and Jin, 2016b

*Data normalized to P10.7=110

4.2. Results: PCA parameterization

Data vs Fit

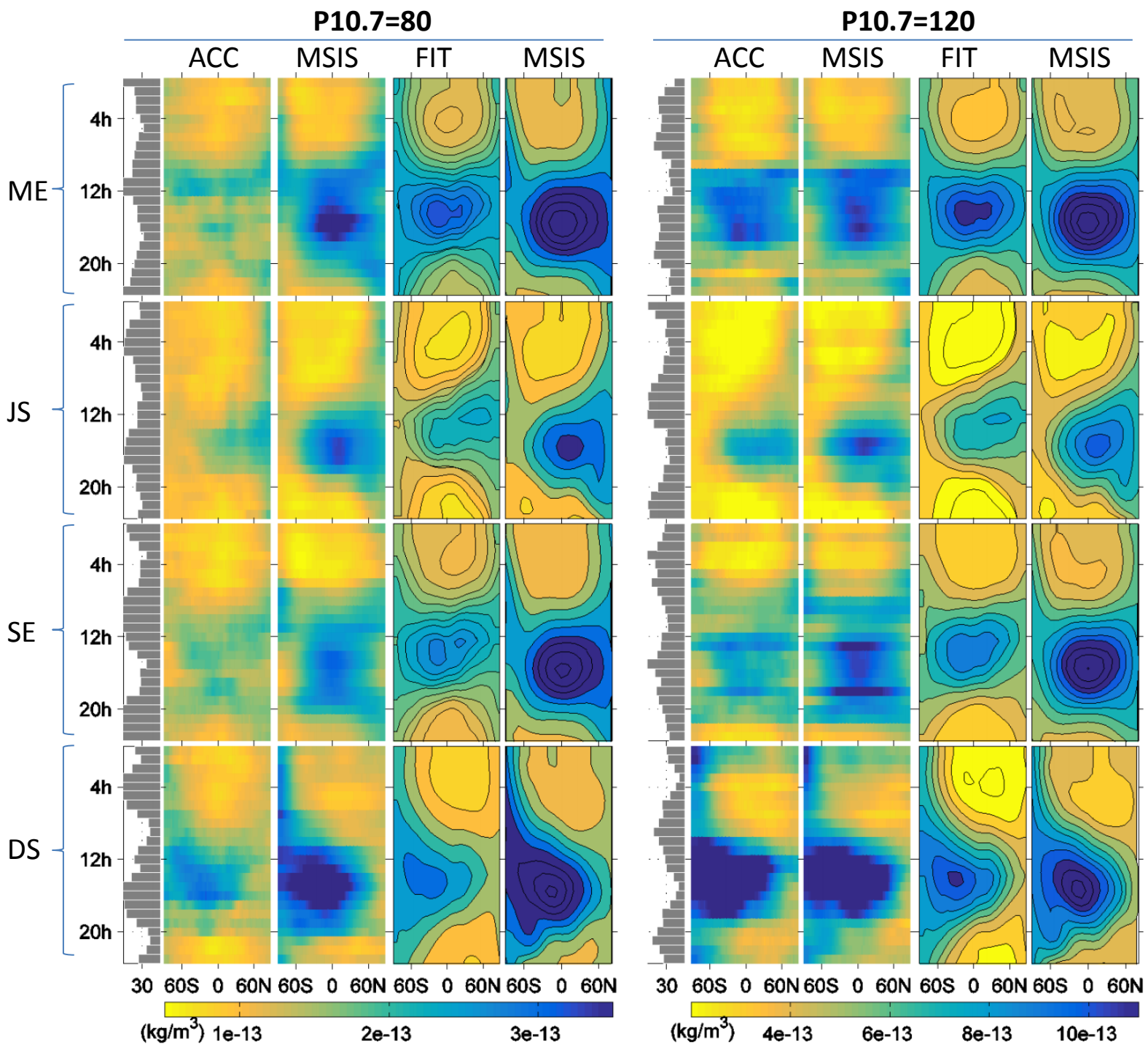


Variance explained	Data - Fit correlation
92 %	96 %
3.5%	93 %
3%	90 %
1.3 %	83 %

*Calabia and Jin, 2017

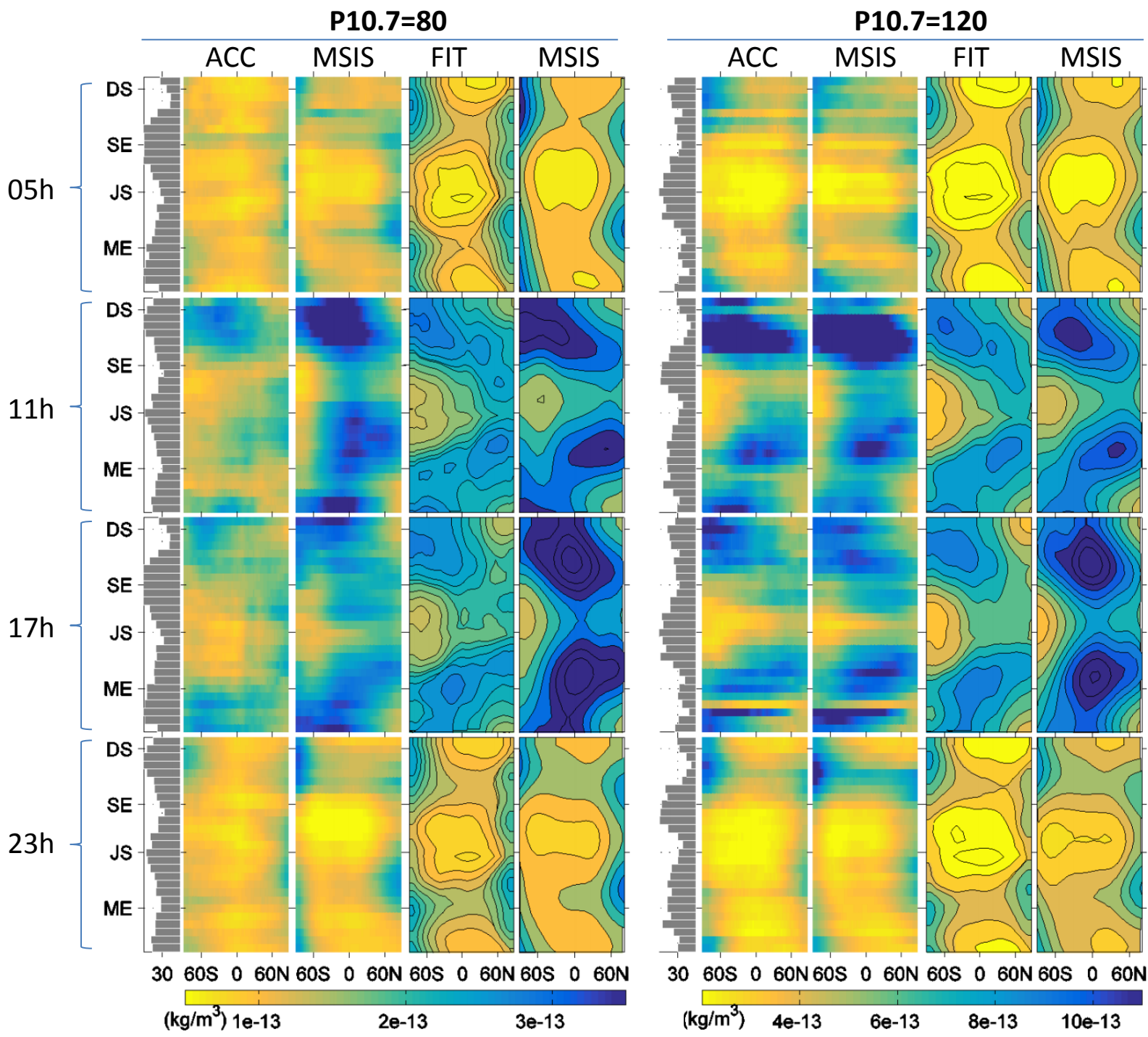
4.2. Results: PCA parameterization

Measurements and models



4.2. Results: PCA parameterization

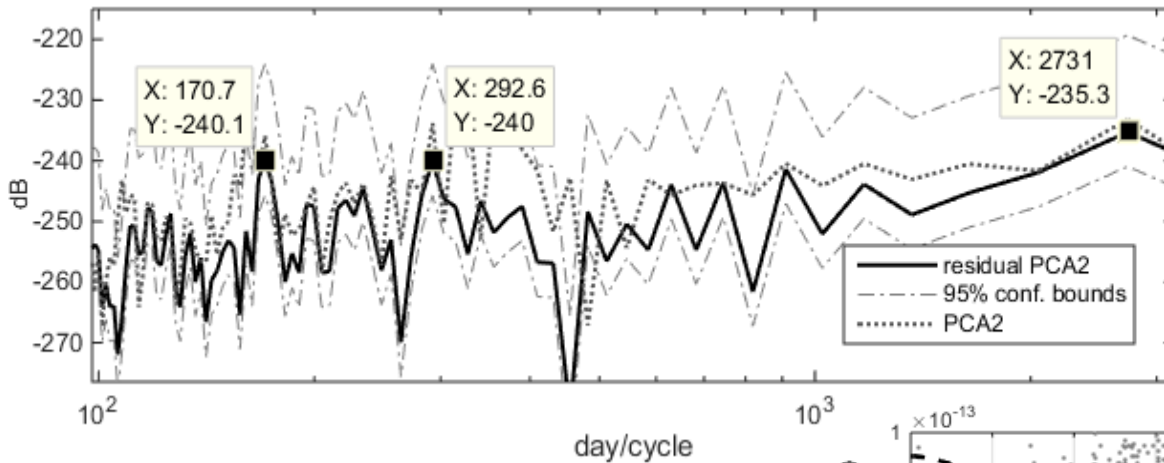
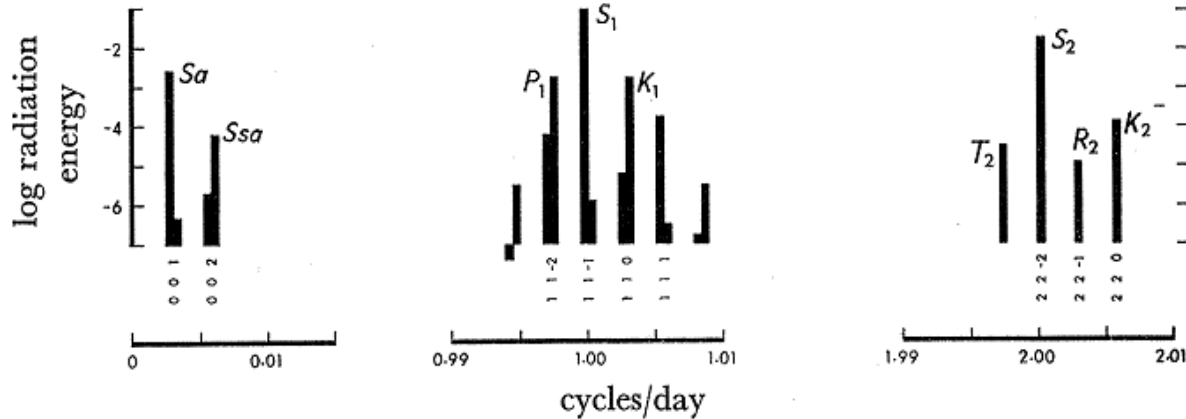
Measurements and models



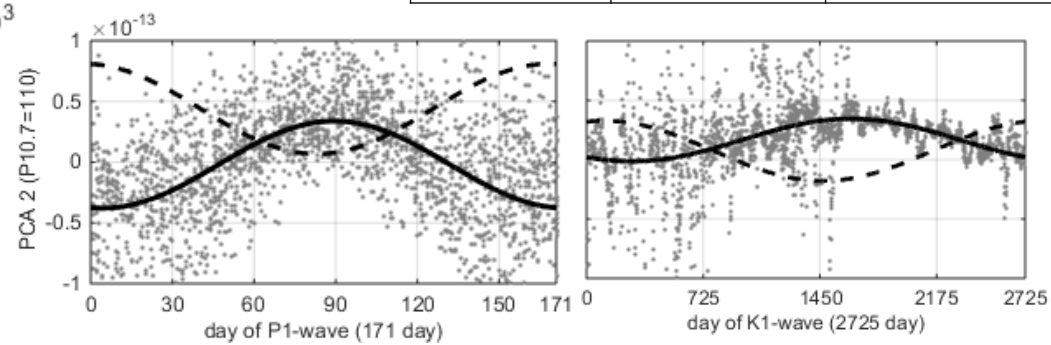
4.3. Results: Residuals analysis

Spectrum of radiational waves

* Radiational tide spectra
(Munk and Cartwright, 1966)

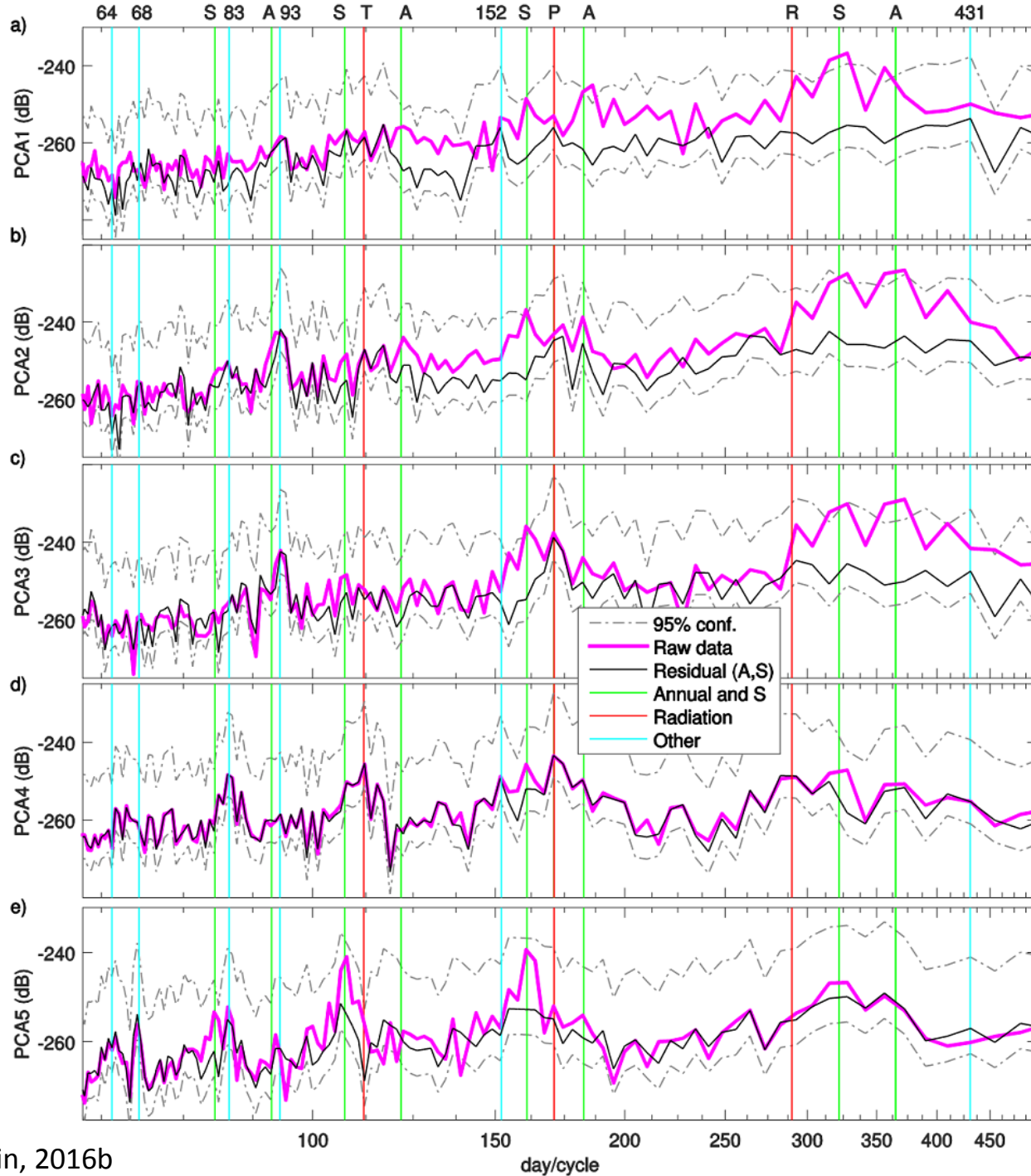


Darwin symbol	Period (day)	Alias period (day)
P1	1.0027454	171.13
S1	1	322
K1	0.9972696	2719.68
K+2	0.9971964	1700
T2	0.5006854	111.74
R2	0.4993165	287.89



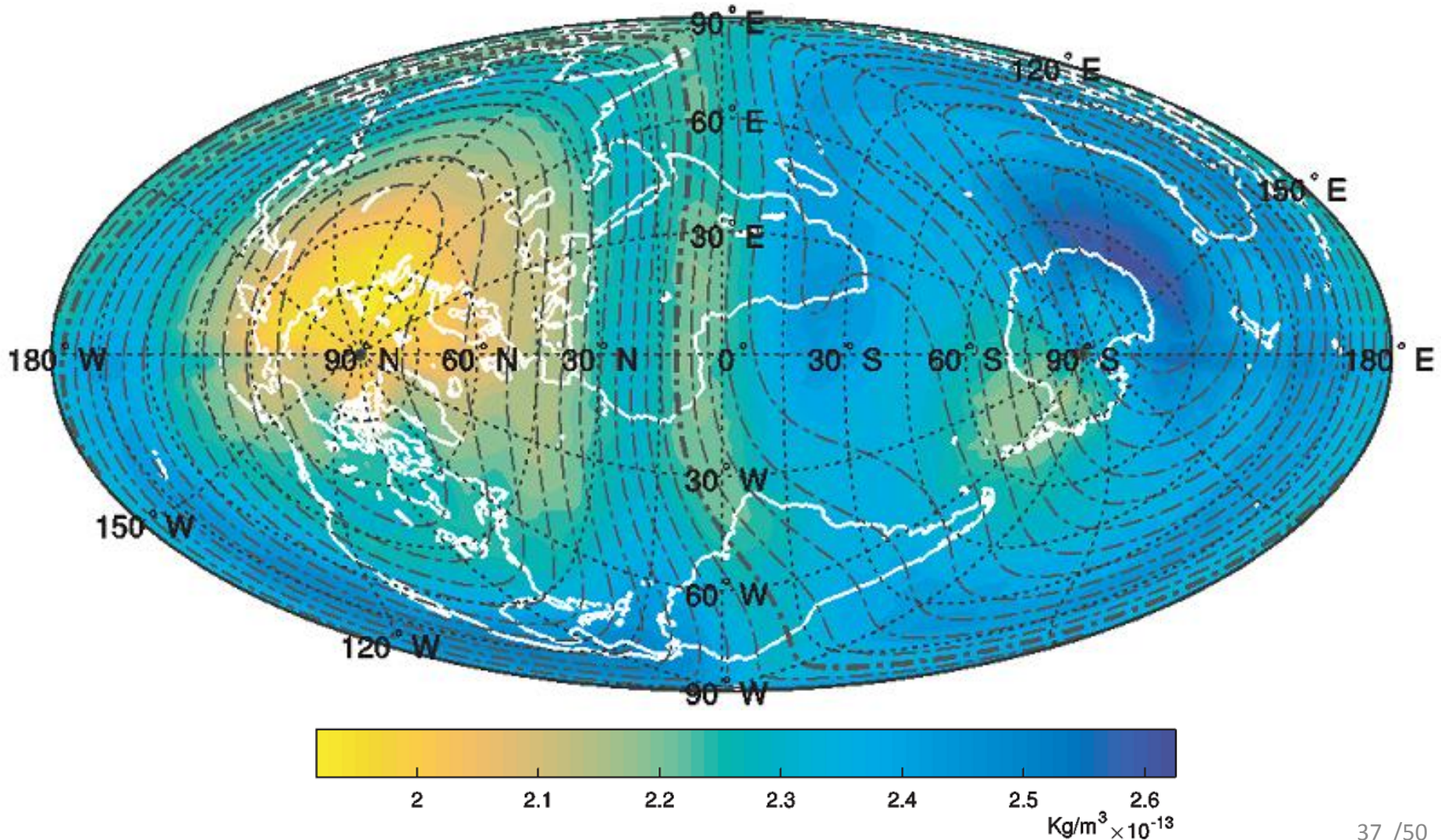
4.3. Results: Residuals analysis

Periodogram



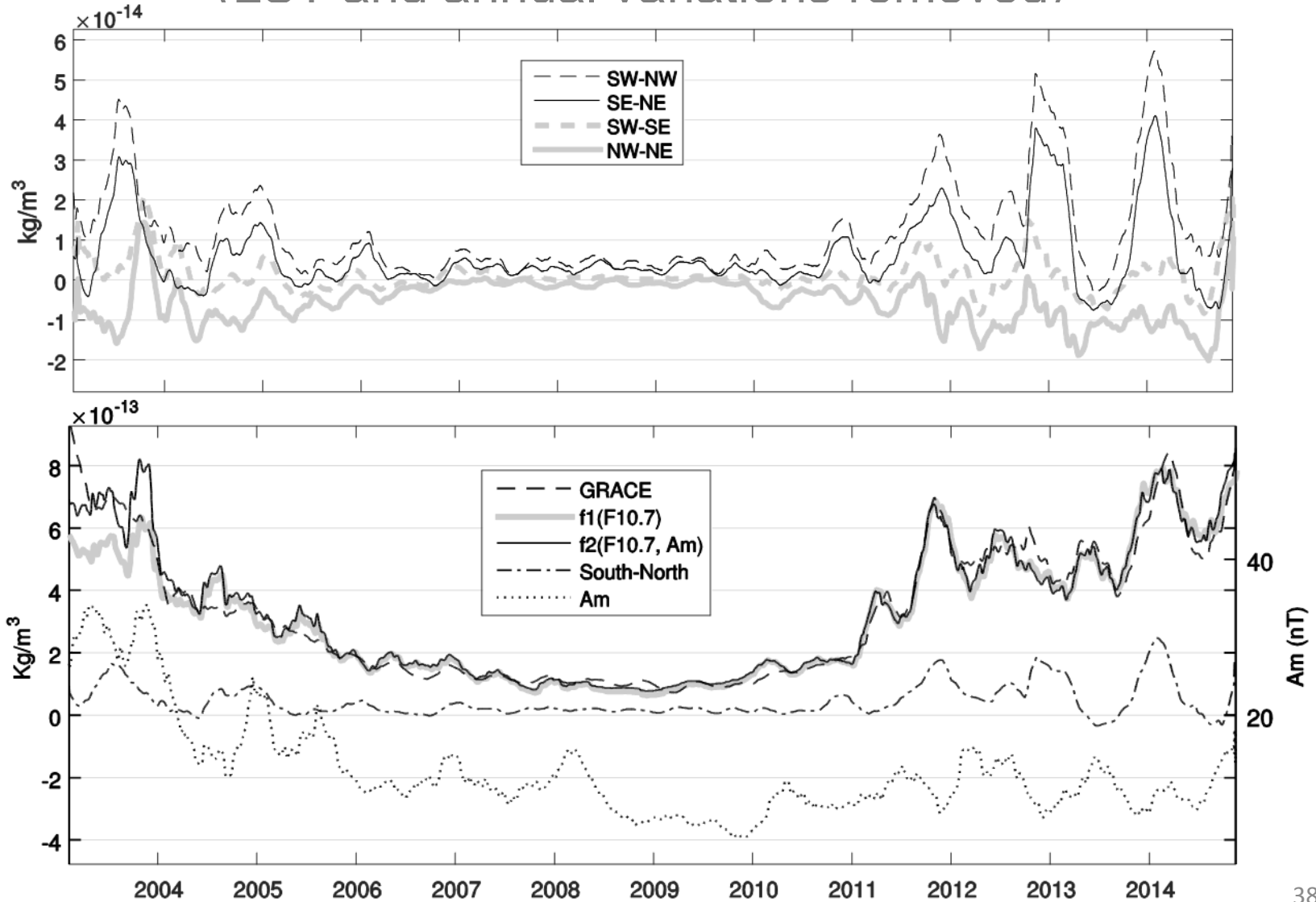
4.4. Results: Global distribution

Averaged thermospheric neutral density (475 Km)
(LST and annual variations removed)



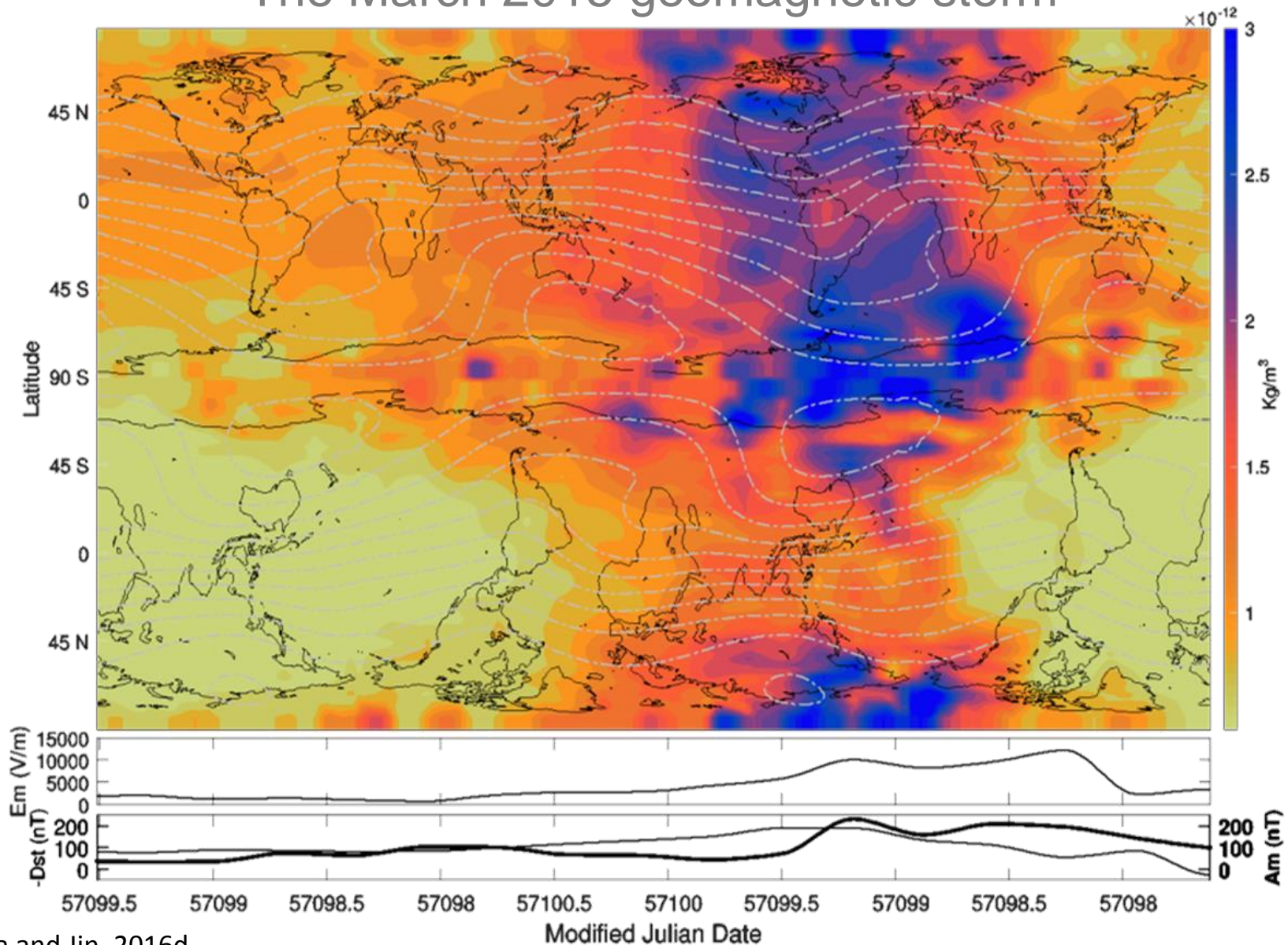
4.4. Results: Long-term trend

Daily mean density (475 Km) 81-day smoothed
(LST and annual variations removed)



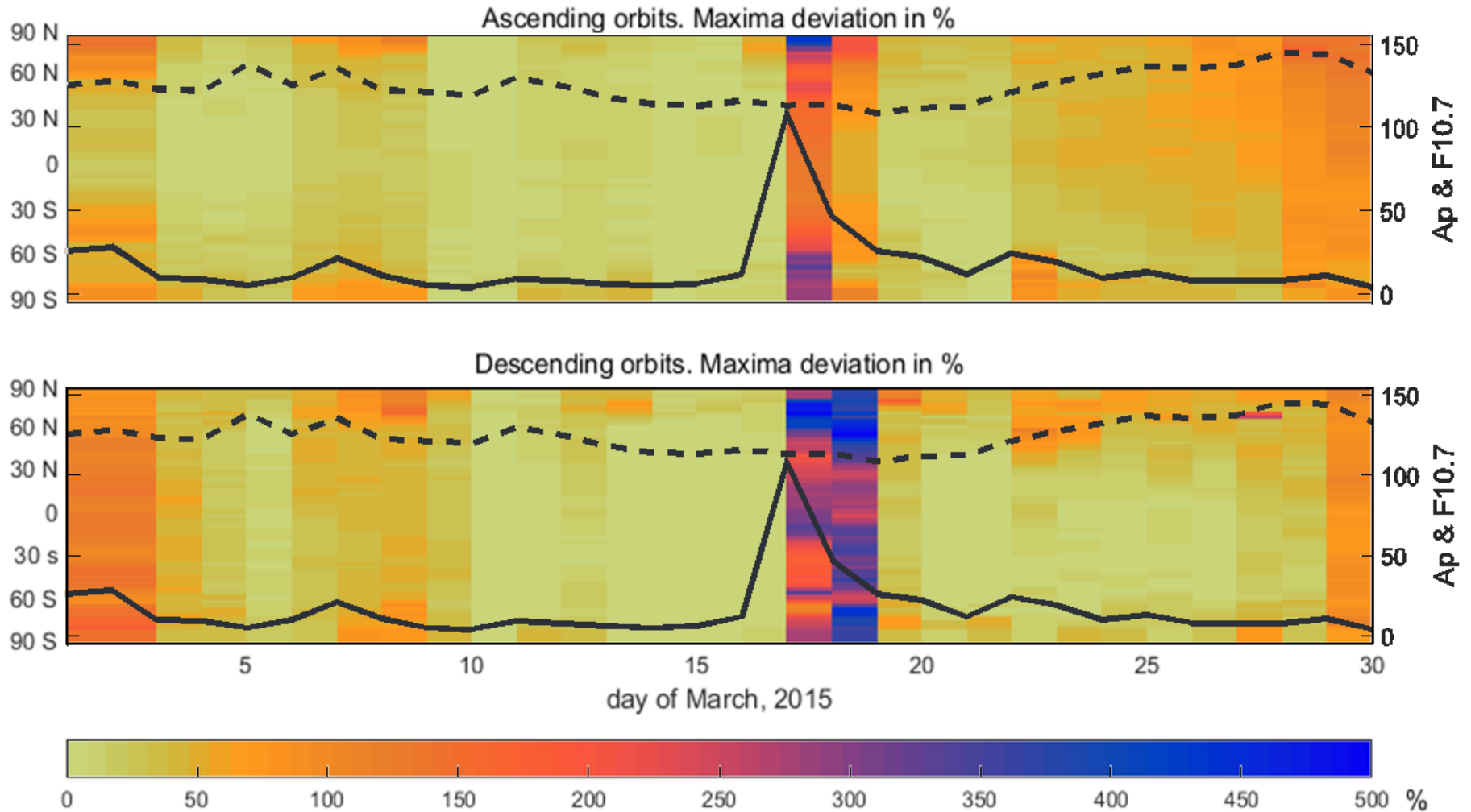
4.5. Results: Geomagnetic storm

The March 2015 geomagnetic storm



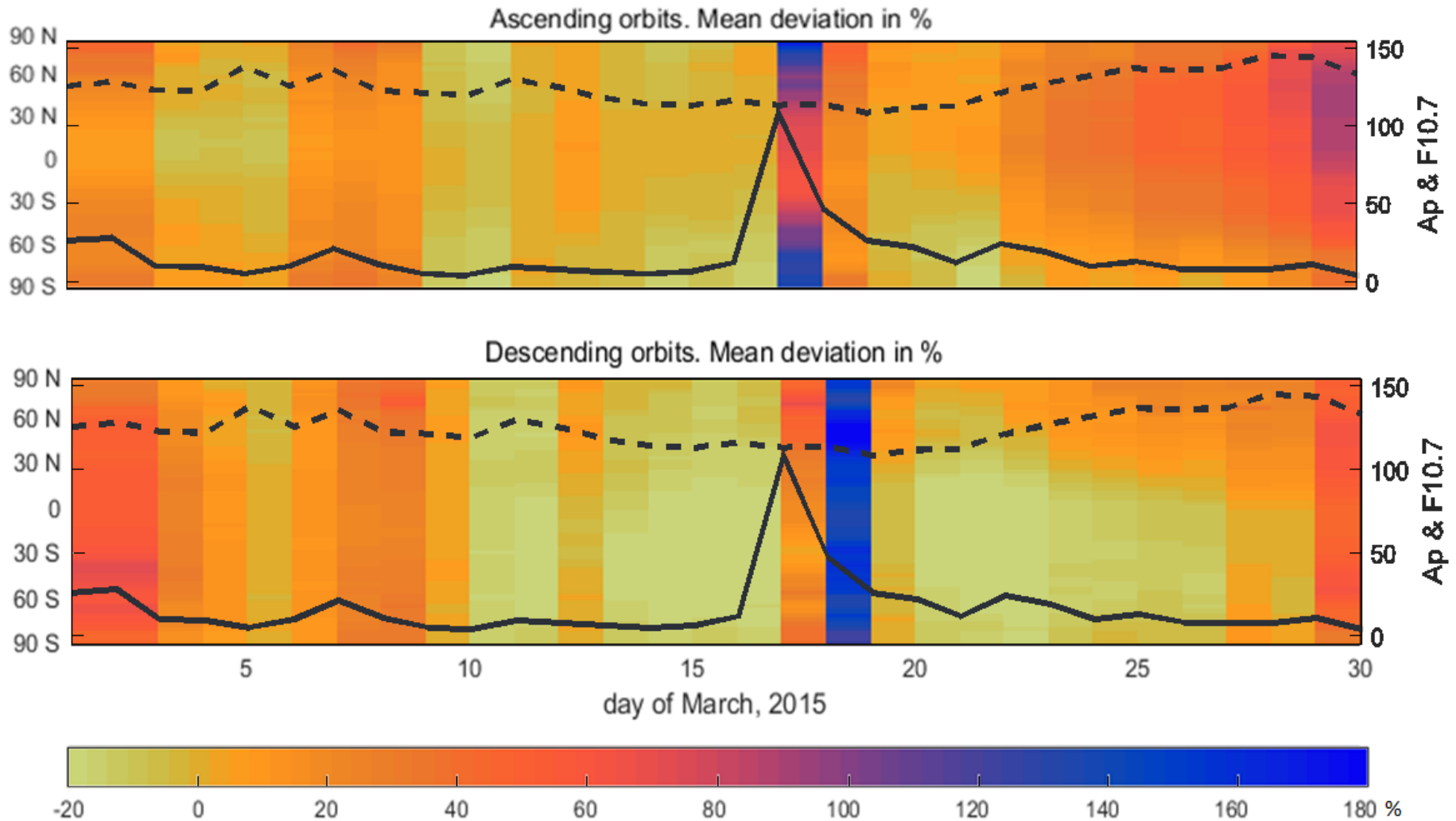
4.5. Results & Discussion

Maxima deviation



4.5. Results & Discussion

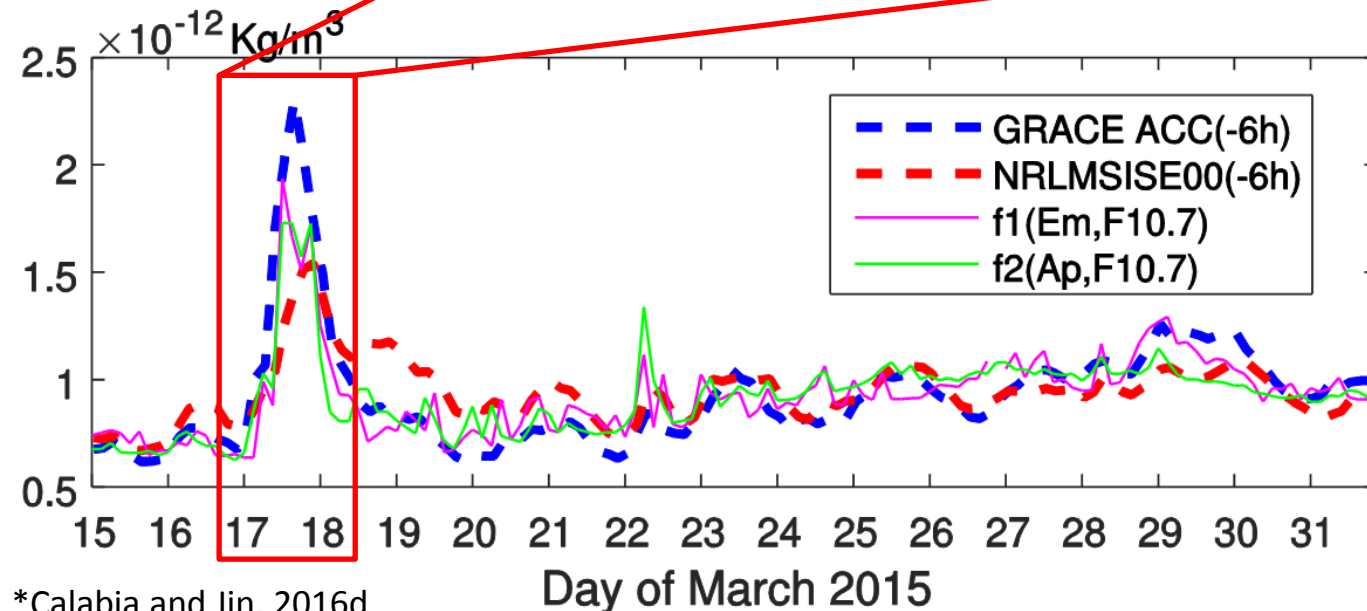
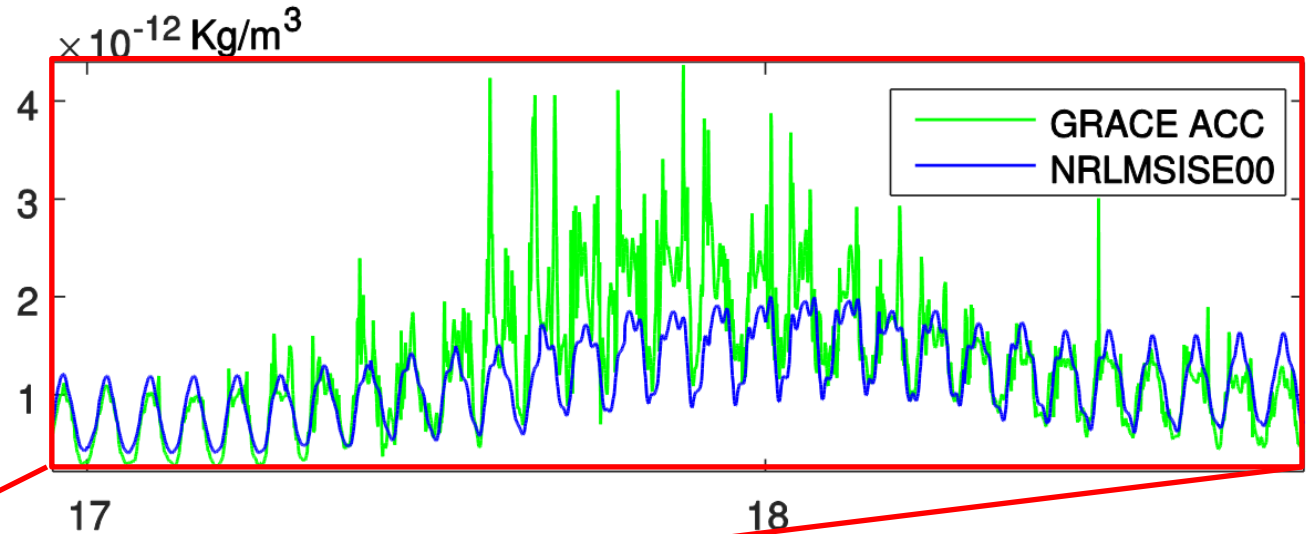
Mean deviation



4.5. Results: Geomagnetic storm

The March 2015 geomagnetic storm

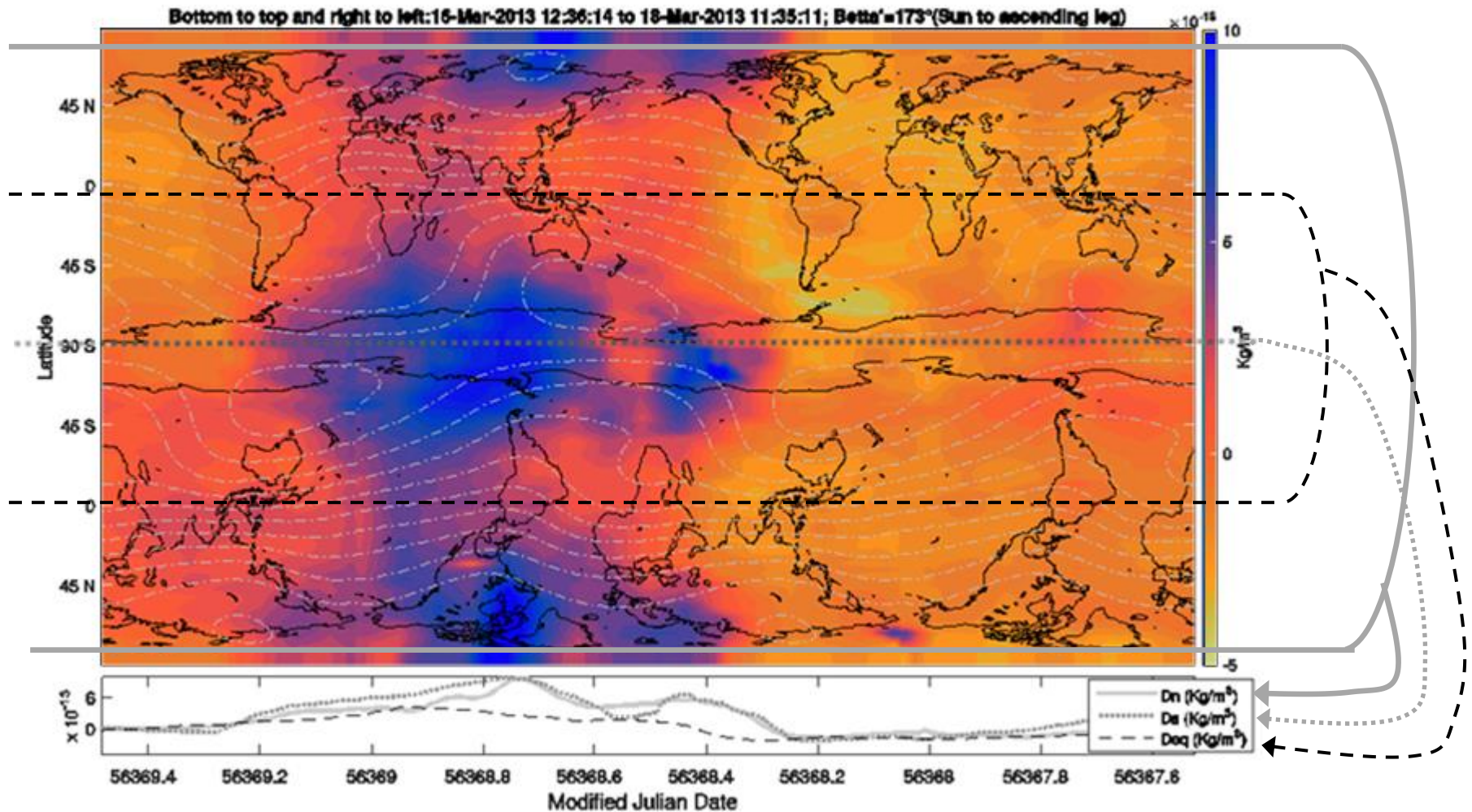
Neutral density
(475 Km) along
GRACE orbit



Mean values per
orbit and
parameterization

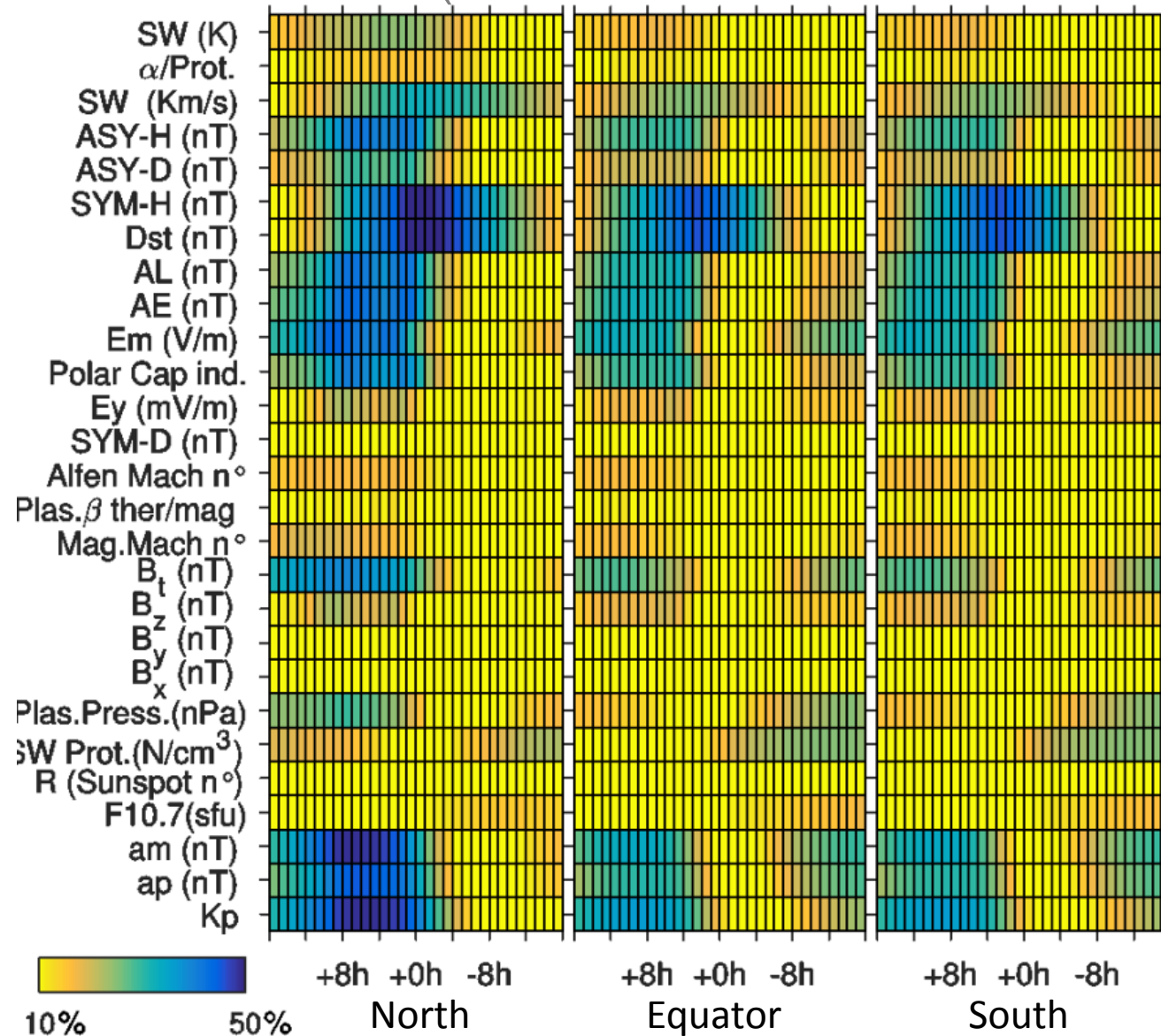
4.5. Results: Geomagnetic storm

Northern, Equatorial, and Southern profiles



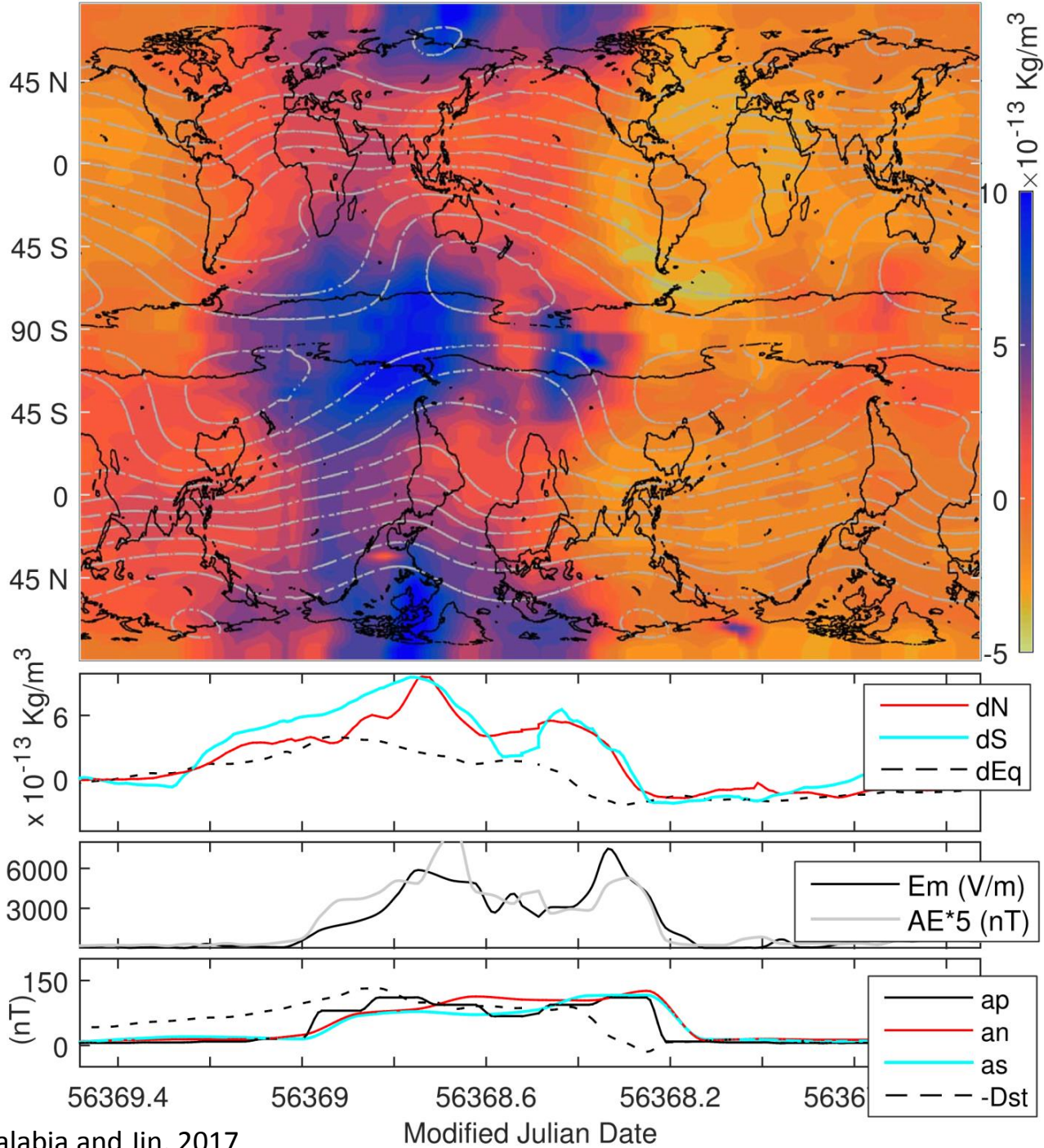
4.5. Results: Geomagnetic storm

Correlation versus delay-times with respect to density variations 2011-2016 (free from annual and LST variations)



4.5. Results: Geomagnetic storm

The March 2013 geomagnetic storm
(LST and annual variations removed)



*Calabia and Jin, 2017

5. Conclusions

- **The new technique to derive non-gravitational accelerations from numerically differentiated POE has shown good agreement with accelerometer measurements, and good results for accelerometer calibration and neutral density estimation.**
- **A new systematic error inherent to the generalized POD scheme has been found in GRACE's and GOCE's solution.**
- **The new PCA-based technique for the spatiotemporal analysis of satellite measurements along orbits has shown great feasibility with very good results.**

5. Conclusions

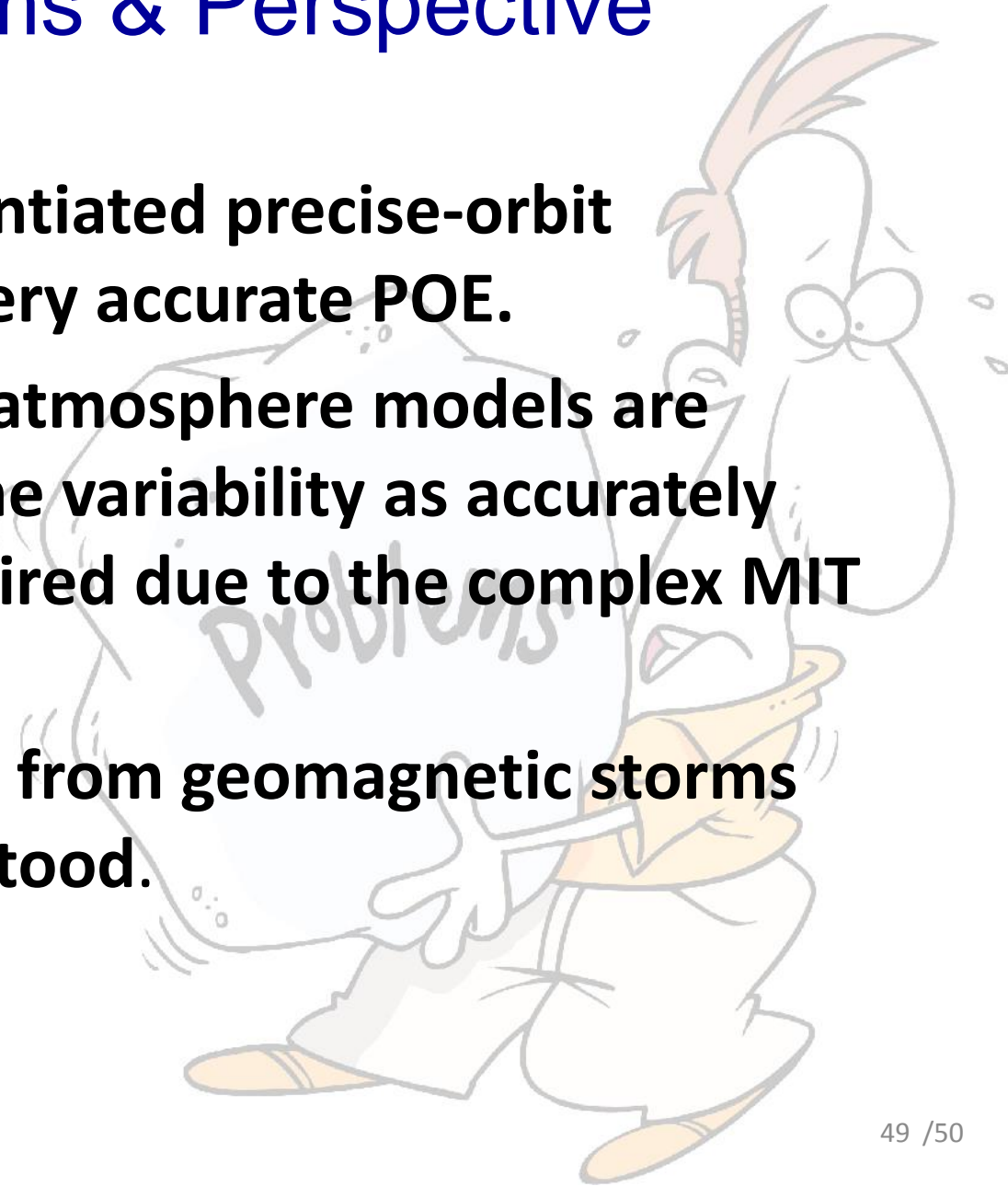
- **Conservative-force anomalies derived from analytical TVG, POE, and accelerometer measurements have shown strong structures at LST and sub-daily frequencies.**
- **A better understanding of thermospheric neutral density distribution and variations is presented.**
 - ✓ **The new model is suitable to represent small scale variations including, e.g., EMA and MDM.**
 - **The residuals have shown periodic contributions at the frequencies of the radiational tides (P1, K, T2, and R2) and at the periods of 83, 93, 152 and 431 days.**

5. Conclusions

- **The long-term distribution shows a alignments with the geomagnetic field, higher density in the southern hemisphere, and two asymmetric cells located in the polar caps.**
- **Thermospheric neutral density variations during geomagnetic storms better correlate to *Dst* index at low latitudes, and to *Em* and *k*-planetary indices at high latitudes.**

6. Problems & Perspective

- **Numerically differentiated precise-orbit velocities require very accurate POE.**
- **The present upper-atmosphere models are unable to predict the variability as accurately and efficiently required due to the complex MIT coupling.**
- **Resulting processes from geomagnetic storms are not well understood.**

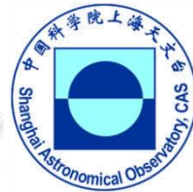


6. Problems & Perspective

- **Study density variations from other missions (e.g., SWARM, GRACE FO) and models.**
- **Modeling of simultaneous measurements in a combined solution of wind and density estimates.**
- **Integrate other techniques (e.g., ultraviolet remote sensing, incoherent scatter radar, atmospheric occultation, Broglio Drag Balance instrument, pressure gauge devices).**



UNIVERSITY OF CHINESE ACADEMY OF SCIENCES
SHANGHAI ASTRONOMICAL OBSERVATORY



THAT'S ALL!

The End

Thank you very much!

See you soon!



Andy